Journal of Computational Physics **169,** 250–301 (2001)
doi:10.1006/jcph.2000.6582, available online at http://www.idealibrary.com on IDEAL®

Interfacial Dynamics for Stokes Flow

C. Pozrikidis

Department of Mechanical and Aerospace Engineering, University of California, San Diego, La Jolla, California 92093-0411
E-mail: cpozrikidis@ucsd.edu, URL: http://stokes.ucsd.edu/c_pozrikidis

Received December 16, 1999; revised June 6, 2000

Theoretical and computational aspects of the method of interfacial dynamics for flow at vanishing Reynolds number are considered. The mathematical formulation relies on the boundary-integral representation that expresses the flow in terms of distributions of Stokes-flow singularities over the interfaces. The densities of the distributions are identified with the jump in the hydrodynamic traction due to interfacial in-plane and transverse tensions, the interfacial velocity, or the strength of a hydrodynamic potential. The numerical procedure involves describing the interfaces in terms of interfacial marker points that reproduce the evolving shapes of the interfaces by global or local interpolation; solving integral equations of the second kind for the interfacial velocity or for the density of a hydrodynamic potential; and computing the motion of the marker points while simultaneously updating interfacial fields relevant to the dynamics, including the concentration of a surfactant and the position of interfacial point particles at an equilibrium configuration. Interfaces exhibiting isotropic tension, elastic tensions, viscous, and incompressible behavior are considered. The mathematical modeling of the tensions and bending moments developing over interfaces with a membrane-like constitution is discussed in the context of the theory of thin shells. To facilitate the numerical implementation, the coupling of the interfacial mechanics to the hydrodynamics by means of interface force and torque balances is formulated in global Cartesian coordinates. Recent progress in the implementation of boundary-element methods is reviewed, and areas for further research are identified.

Key Words: Stokes flow; boundary-integral methods; interfaces; integral equations; suspensions; emulsions.

CONTENTS

0021-9991/01 $35.00

1. INTRODUCTION

In two seminal papers, Jawson [59] and Symm [183] demonstrated that the integral equations relating the boundary values of a harmonic function to the boundary distribution of its normal derivative may be solved accurately and economically using relatively simple numerical methods. In the nearly four decades that have elapsed, their approach has been extended and generalized to encompass a multitude of problems in several branches of science and engineering. The new methodology has spawned the well-established class of boundary-element methods founded by Brebbia [17] with initial emphasis on potential-field theory and elastostatics. Numerical solutions of the boundary-integral equation for Stokes flow were first presented by Youngren and Acrivos [200] with reference to flow past a rigid particle. A growing body of literature on boundary-integral-equation methods and their derivative class of boundary-element methods for low-Reynolds-number flow has been established since that time, as reviewed by Kim and Karrila [66] and Pozrikidis [127].

The boundary-integral representation expresses the solution of a linear elliptic partial differential equation in terms of generalized distributions of singularities over boundaries. The goal of the numerical method is to generate the densities of the distributions by solving an integral equation that descends from the boundary-integral representation. If jump-conditions across the interface between two solution domains instead of boundary conditions are specified, the two integral representations on either side of the interface may be combined into a unified form. The coupling can be done either before or after the integral equations have been discretized to yield algebraic forms. The first approach produces elegant and physically appealing representations in terms of geometrical shapes and material properties, and thereby allows for insightful interpretations. For example, in the case of fluid flow past an interface with uniform surface tension, the integral representation expresses the flow variables in terms of the interfacial mean curvature, and the overall formulation effectively implements a dynamical law for the self-induced motion of the interface driven by its curvature.

Integral equations for Stokes flow involving the jump in the traction across an interface were first derived by Youngren and Acrivos [201] and Rallison and Acrivos [149] with reference to the deformation of a bubble or drop subject to an axisymmetric elongational flow. In subsequent years, considerable progress has been made on several fronts: Generalization of the integral formulations with respect to interfacial properties and flow configuration; theoretical analysis of the properties of the integral equations; and implementation of efficient numerical procedures for simulating complex interfacial motions. Advanced interfacial properties and many-body systems with applications in materials science, chemical engineering, geophysics, and biomechanics have also been considered.

The mathematical foundation of, and early work on, boundary-integral methods for Stokes flow in the presence of interfaces was reviewed by Pozrikidis [127]; the present article serves as an update. Recent and some original theoretical developments are discussed, new types of interfacial properties are considered, progress on numerical implementation is reported, and topics for further research are identified. Attention is focused exclusively on Newtonian

fluids and on quasi-steady flow at vanishing Reynolds number. The articles by Toose *et al.* [186], Occhialini *et al.* [116], and Khayat [63] are points of entry into the rather limited but growing literature of boundary-integral methods for non-Newtonian fluids and flow at nonzero Reynolds numbers.

2. INTEGRAL REPRESENTATIONS AND INTEGRAL EQUATIONS

Consider the motion of a collection of deformable particles, including bubbles, drops, and capsules, consisting of the same or different Newtonian fluids, suspended in another ambient Newtonian fluid. In the limit of vanishing Reynolds number *Re*, where *Re* is defined with respect to the typical particle size, inertial forces are insignificant, and the motion of the fluid inside and outside the particles is governed by the linear equations of Stokes flow (e.g., Pozrikidis [127, 133]).

In this section, we review boundary-integral formulations that provide us with a basis for computing the instantaneous distribution of the velocity over the interfaces, and for evaluating the velocity and the pressure at any point in the flow.

2.1. *Two-Dimensional Flow*

To begin, we consider a suspension of N two-dimensional particles evolving under the influence of an imposed flow, as illustrated in Fig. 1a. Requiring that the velocity be continuous across the interfaces, and following a standard methodology (e.g., Pozrikidis, [127, Chap. 5]), we find that the velocity at a point $\mathbf{x}_0$ that is located within the suspending fluid is given by the integral representation

$$u_j(\mathbf{x}_0) = u_j^{\infty}(\mathbf{x}_0) - \frac{1}{4\pi\mu_s}\sum_{m=1}^{N}\int_{C_m} \Delta\tilde{f}_i(\mathbf{x})G_{ij}(\mathbf{x},\mathbf{x}_0)\,dl(\mathbf{x}) + \frac{1}{4\pi}\sum_{m=1}^{N}(1-\lambda_m)\int_{C_m} u_i(\mathbf{x})T_{ijk}(\mathbf{x},\mathbf{x}_0)n_k(\mathbf{x})\,dl(\mathbf{x}), \tag{2.1}$$

where $\mathbf{u}^{\infty}$ is the imposed velocity prevailing in the absence of the particles, C_m stands for the interface of the mth particle, l is the arc length along C_m, μ_s is the viscosity of the ambient suspending fluid, μ_m is the viscosity of the mth particle, $\lambda_m = \mu_m/\mu_s$ is the corresponding viscosity ratio, and $\mathbf{n}$ is the unit vector normal to the interfaces pointing into the ambient fluid. In the case of flow extending to infinity, the boundary-integral representation must be derived carefully to avoid the occurrence of Stokes's paradox where far from the particles the velocity diverges at a logarithmic rate.

The first integral on the right-hand side of (2.1) is the single-layer hydrodynamic potential, and the second integral is the double-layer hydrodynamic potential of Stokes flow. The kernels $\mathbf{G}$ and $\mathbf{T}$ are the Green's functions of Stokes flow representing, respectively, the velocity and stress field due to a point force in solitary or periodic configuration. We have assumed that the Green's function for the velocity conforms with the specified periodicity of the flow and vanishes over the solid boundaries of the flow. For example, if the flow is bounded by the rigid boundary C_{B}, then the velocity Green's function $\mathbf{G}$ is required to vanish when either the point force or the field point is located on C_{B}; otherwise, additional integrals over boundaries arise.

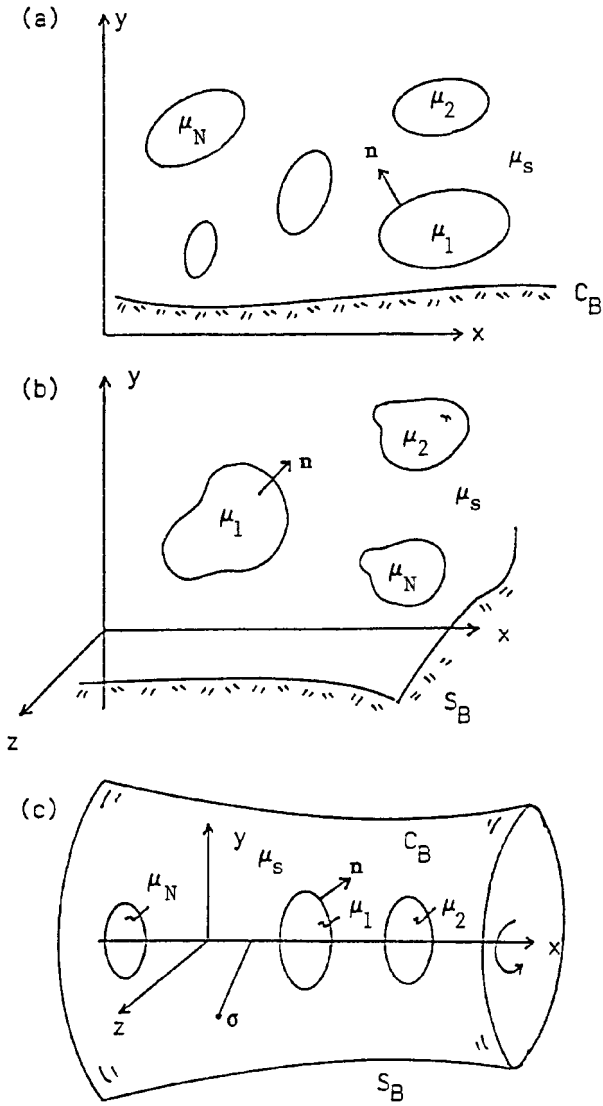

FIG. 1. Schematic illustration of a suspension of capsules in (a) two-dimensional, (b) three-dimensional, and (c) axisymmetric flow.

The density of the distribution of the single-layer potential, denoted by $\Delta\tilde{\mathbf{f}}$, is the modified jump in the traction across the particle interface, defined as

$$\Delta\tilde{\mathbf{f}} \equiv \tilde{\mathbf{f}}^{(\mathrm{s})} - \tilde{\mathbf{f}}^{(\mathrm{p})} = \left(\tilde{\sigma}^{(\mathrm{s})} - \tilde{\sigma}^{(\mathrm{p})}\right) \cdot \mathbf{n}, \tag{2.2}$$

where $\tilde{\sigma}$ is the Newtonian stress tensor modified to incorporate the presence of a conservative body force, the superscript (s) denotes the ambient suspending fluid, and the superscript (p) denotes a particle. For example, if the body force is due to gravity, then $\tilde{\sigma} = \sigma + \rho(\mathbf{g}\cdot\mathbf{x})\mathbf{I}$, where $\mathbf{g}$ is the acceleration of gravity and $\mathbf{I}$ is the identity matrix. Accordingly,

$$\begin{aligned}\Delta\tilde{\mathbf{f}} \equiv &= \left\{\left[\sigma^{(\mathrm{s})} + \rho^{(\mathrm{s})}(\mathbf{g}\cdot\mathbf{x})\mathbf{I}\right] - \left[\sigma^{(\mathrm{p})} + \rho^{(\mathrm{p})}(\mathbf{g}\cdot\mathbf{x})\mathbf{I}\right]\right\} \cdot \mathbf{n} \\ &= \Delta\mathbf{f} + \left(\rho^{(\mathrm{s})} - \rho^{(\mathrm{p})}\right)(\mathbf{g}\cdot\mathbf{x})\mathbf{n},\end{aligned} \tag{2.3}$$

where

$$\Delta \mathbf{f} \equiv \mathbf{f}^{(\mathrm{s})} - \mathbf{f}^{(\mathrm{p})} = \left(\sigma^{(\mathrm{s})} - \sigma^{(\mathrm{p})}\right) \cdot \mathbf{n} \tag{2.4}$$

is the physical jump in traction determined by the properties of the interface, as will be discussed in Sections 3–7.

For a point $\mathbf{x}_0$ that lies inside the qth particle, where $q = 1, \ldots, N$, the velocity is given by the integral representation (2.1), except that all terms on the right-hand side are divided by the viscosity ratio λ_q. Taking the limit as the point $\mathbf{x}_0$ approaches the interface of the qth particle, and expressing the limit of the double-layer potential in terms of its principal value, we derive the following Fredholm integral equation of the second kind for the interfacial velocity (also known as the boundary-integral equation),

$$u_j(\mathbf{x}_0) = \frac{2}{1+\lambda_q}\left[u_j^{\infty}(\mathbf{x}_0) - \frac{1}{4\pi\mu_s}\sum_{m=1}^{N}\int_{C_m} \Delta \tilde{f}_i(\mathbf{x}) G_{ij}(\mathbf{x}, \mathbf{x}_0)\, dl(\mathbf{x}) + \frac{1}{4\pi}\sum_{m=1}^{N}(1-\lambda_m)\int_{C_m}^{\mathrm{PV}} u_i(\mathbf{x}) T_{ijk}(\mathbf{x}, \mathbf{x}_0) n_k(\mathbf{x})\, dl(\mathbf{x})\right], \tag{2.5}$$

where PV denotes the principal value (e.g., Pozrikidis [127]). The solution of this integral equation is the cornerstone of computational methods for interfacial dynamics in Stokes flow.

An alternative formulation in terms of the vorticity and the stream function is possible in the case of two-dimensional flow or axisymmetric flow, to be considered later in this section [62, 71]. The present formulation in terms of the velocity and the traction, however, has the advantage that it may readily be extended to three dimensions and allows the straightforward implementation of different types of interfacial behavior.

2.2. *Three-Dimensional Flow*

Next, we consider a suspension of N three-dimensional particles evolving under the influence of an imposed flow, as illustrated in Fig. 1b. The counterpart of the boundary-integral representation (2.1) is

$$u_j(\mathbf{x}_0) = u_j^{\infty}(\mathbf{x}_0) - \frac{1}{8\pi\mu_s}\sum_{m=1}^{N}\int_{D_m} \Delta \tilde{f}_i(\mathbf{x}) G_{ij}(\mathbf{x}, \mathbf{x}_0)\, dS(\mathbf{x}) + \frac{1}{8\pi}\sum_{m=1}^{N}(1-\lambda_m)\int_{D_m} u_i(\mathbf{x}) T_{ijk}(\mathbf{x}, \mathbf{x}_0) n_k(\mathbf{x})\, dS(\mathbf{x}), \tag{2.6}$$

where D_m stands for the interface of the mth particle, dS is an infinitesimal surface area of D_m, and the rest of the symbols were defined in Section 2.1. For a point $\mathbf{x}_0$ that lies inside the qth particle, where $q = 1, \ldots, N$, the velocity is given by the integral representation (2.6) except that all terms on the right-hand side are divided by the viscosity ratio λ_q. The counterpart of the integral equation (2.5) is

$$u_j(\mathbf{x}_0) = \frac{2}{1+\lambda_q}\left[u_j^{\infty}(\mathbf{x}_0) - \frac{1}{8\pi\mu_s}\sum_{m=1}^{N}\int_{S_m} \Delta \tilde{f}_i(\mathbf{x}) G_{ij}(\mathbf{x}, \mathbf{x}_0)\, dS(\mathbf{x}) + \frac{1}{8\pi}\sum_{m=1}^{N}(1-\lambda_m)\int_{S_m}^{\mathrm{PV}} u_i(\mathbf{x}) T_{ijk}(\mathbf{x}, \mathbf{x}_0) n_k(\mathbf{x})\, dS(\mathbf{x})\right], \tag{2.7}$$

where the point $\mathbf{x}_0$ lies at the interface of the qth particle, $q = 1, \ldots, N$, and PV denotes the principal value of the double-layer integral.

2.3. *Axisymmetric Flow*

As a special case of three-dimensional flow, we consider a suspension of N coaxial axisymmetric particles evolving under the influence of an imposed axisymmetric flow, possibly in the presence of axisymmetric boundaries, as illustrated in Fig. 1c. The counterpart of the integral representation (2.1) is

$$u_\alpha(\mathbf{x}_0) = u_\alpha^\infty(\mathbf{x}_0) - \frac{1}{8\pi\mu_s}\sum_{m=1}^{N}\int_{C_m} G_{\alpha\beta}(\mathbf{x},\mathbf{x}_0)\Delta\tilde{f}_\beta(\mathbf{x})\,dl(\mathbf{x}) + \frac{1}{8\pi}\sum_{m=1}^{N}(1-\lambda_m)\int_{C_m} u_\beta(\mathbf{x})T_{\alpha\beta\gamma}(\mathbf{x},\mathbf{x}_0)n_\gamma(\mathbf{x})\,dl(\mathbf{x}), \tag{2.8}$$

where Greek symbols stand for x or σ denoting, respectively, the x position and the distance from the x axis, as illustrated in Fig. 1c, C_m stands for the trace of the interface of the mth particle in a meridional plane of constant angle φ, and the rest of the symbols were defined in Section 2.1.

For a point $\mathbf{x}_0$ that lies inside the qth particle, where $q = 1, \ldots, N$, the velocity is given by the integral representation (2.8) except that all terms on the right-hand side are divided by the viscosity ratio λ_q. The counterpart of the integral equation (2.5) is

$$u_\alpha(\mathbf{x}_0) = \frac{2}{1+\lambda_q}\left[u_\alpha^\infty(\mathbf{x}_0) - \frac{1}{8\pi\mu_s}\sum_{m=1}^{N}\int_{C_m} G_{\alpha\beta}(\mathbf{x},\mathbf{x}_0)\Delta\tilde{f}_\beta(\mathbf{x})\,dl(\mathbf{x}) + \frac{1}{8\pi}\sum_{m=1}^{N}(1-\lambda_m)\int_{C_m}^{\mathrm{PV}} u_\alpha(\mathbf{x})T_{\alpha\beta\gamma}(\mathbf{x},\mathbf{x}_0)n_\gamma(\mathbf{x})\,dl(\mathbf{x})\right], \tag{2.9}$$

where the point $\mathbf{x}_0$ lies at the interface of the qth particle, $q = 1, \ldots, N$.

2.4. *Single-Layer Representation*

We have discussed integral representations of Stokes flow in terms of combined single-layer and double-layer potentials with physical density distributions. To evaluate the velocity at a certain point in the flow, we must first assess whether the point lies in the interior or exterior of a particle, and then use the corresponding integral representation. Locating the position of a point relative to the interfaces can be done by several methods with varying degrees of reliability and sophistication (e.g., Pozrikidis [136, Chap. 1]). The additional effort, however, imposes an undesirable computational burden especially when a large number of evaluations are required.

To circumvent this difficulty, we express the flow in terms of a single-layer potential with an *a priori* unknown density distribution. For example, in the case of three-dimensional flow, we write

$$u_i(\mathbf{x}_0) = u_i^\infty(\mathbf{x}_0) - \sum_{m=1}^{N}\int_{D_m} G_{ij}(\mathbf{x}_0,\mathbf{x})\chi_j(\mathbf{x})\,dS(\mathbf{x}), \tag{2.10}$$

where χ is the density of the single-layer potential, and the point $\mathbf{x}_0$ lies inside or outside a particle (Pozrikidis [124; 127, p. 145]). Straightforward analysis shows that χ satisfies the integral equation of the second kind

$$\chi_i(\mathbf{x}_0) = \frac{2}{8\pi\mu_s(1+\lambda_q)}\left[(1-\lambda_q)\, f_i^{\infty}(\mathbf{x}_0) - \Delta\tilde{f}_i(\mathbf{x}_0) + \sum_{m=1}^{N}(1-\lambda_m)\int_{D_m}^{\mathrm{PV}} T_{ijk}(\mathbf{x}_0,\mathbf{x})\,\chi_j(\mathbf{x}_0) n_k(\mathbf{x}_0)\, dS(\mathbf{x})\right], \tag{2.11}$$

where the point $\mathbf{x}_0$ is located at the qth interface, $q = 1, \ldots, N$, and $f_i^{\infty} = \sigma_{ij}^{\infty} n_j$ is the traction of the incident flow. The principal-value integral on the right-hand side of (2.11) is the adjoint of the double-layer potential shown on the right-hand side of (2.7).

2.5. *Green's Functions*

It was mentioned earlier that the use of a Green's function that conforms with the periodicity of the flow and whose induced velocity vanishes over the solid boundaries of the flow considerably simplifies the integral representation and facilitates the solution of the integral equations. Green's functions for a broad range of flows have been developed and reviewed by several authors including Davis [28], Pozrikidis [127, 132], Maul and Kim [104], and Coulliette and Pozrikidis [25]. Subroutines that evaluate several families of Green's functions for two-dimensional, axisymmetric, and three-dimensional flow are available in the fluid dynamics software library FDLIB [139].

When a large number of evaluations are required, it is expedient to tabulate properly desingularized components of the Green's function with respect to dimensionless arguments, and then compute them by interpolation [91, 25, 81, 22]. The interpolation, however, must be sufficiently accurate; otherwise the method of successive substitutions for solving the integral equations discussed in Section 2.6 may fail, and the interfaces may artificially cross during the motion.

2.6. *Properties of the Integral Equations*

The properties of the integral equations of the second kind depend on the values of the viscosity ratios λ_m and on the choice of the Green's function. When all interfaces are closed and all viscosity ratios are equal, the integral equations have a unique solution as long as none of the fluids is inviscid [66, 124]. Moreover, the solution may be found by the method of successive substitutions, and deflation may be implemented to expedite convergence. Theoretical analyses of the integral equations for other flow configurations have been carried out by several authors including Power [120, 121, 122], Van de Vorst [192], Pozrikidis [138], and Primo *et al.* [146, 147].

3. INTERFACES WITH ISOTROPIC TENSION

Differences in the magnitude of the attractive forces between the molecules of two immiscible species on either side of an interface cause the development of isotropic surface tension γ (e.g., Adamson [1]). Heating and the presence of surfactants alter the strength of

these forces and render the surface tension a function of temperature and local surfactant concentration. As the temperature or the surfactant concentration is reduced, the surface tension is raised; when the temperature reaches the critical point, the surface tension vanishes. Tangential surface-tension gradients generate hydrodynamic tractions identified as Marangoni stresses that may have a significant influence on the structure of the flow and on the deformation of an interface.

3.1. *Jump in the Traction across an Interface*

Consider an interfacial patch enclosed by the contour C, as illustrated in Fig. 2. A force balance over the patch requires

$$\int_{\text{Patch}} \left(\sigma^{(\text{s})} - \sigma^{(\text{p})}\right) \cdot \mathbf{n}\, dS + \int_C \gamma \mathbf{b}\, dl = \mathbf{0}, \tag{3.1}$$

where $\mathbf{b} = \mathbf{t} \times \mathbf{n}$ is a unit vector that is tangential to the interface and lies in a plane that is normal to C, as depicted in Fig. 2, $\mathbf{t}$ is the unit vector tangential to C, and l is the arc length along C. If the interface is described by the equation $G(\mathbf{x}, t) = 0$, where G is a generally time-dependent function, then the unit normal vector is given by $\mathbf{n} = \nabla G/|\nabla G|$. This expression allows us to extend the domain of definition of the normal vector off the plane of the interface and into the whole three-dimensional space. Applying Stokes' theorem to convert the contour integral to a surface integral on the right-hand side of (3.1), and letting the size of the patch become infinitesimal, we find that the jump in hydrodynamic traction across the interface is given by

$$\Delta \mathbf{f} = \left(\sigma^{(\text{s})} - \sigma^{(\text{p})}\right) \cdot \mathbf{n} = \gamma 2\kappa_m \mathbf{n} - \mathbf{P} \cdot \nabla \gamma, \tag{3.2}$$

where $\kappa_m = \frac{1}{2}\nabla \cdot \mathbf{n}$ is the mean curvature, and $\mathbf{P} = \mathbf{I} - \mathbf{nn}$ is the tangential projection operator (e.g., Pozrikidis [127, p. 148]). The two terms on the right-hand side of (3.2) express, respectively, the normal and tangential components of the jump in traction. An alternative derivation of (3.2) will be presented in Section 4 in a more general framework.

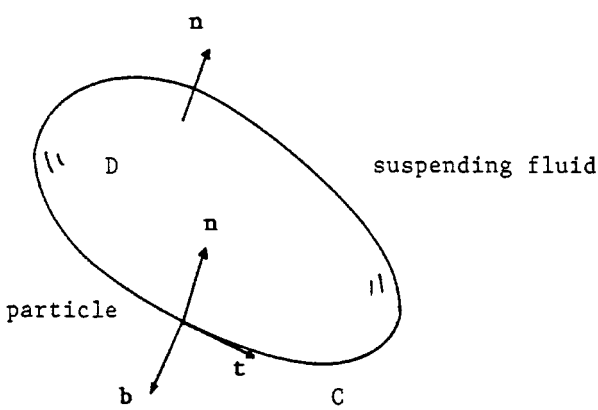

FIG. 2. Force and torque balances are performed over a section of an interface.

3.2. *Double-Layer Representation*

In the Appendix, we show that two arbitrary vector functions **A** and **B** defined in three-dimensional space satisfy the integral identity (A.4), where the domain of integration D is a closed surface. Let us identify D with the interface of a particle, extend the domain of definition of the normal vector and surface tension into the whole space, and set

$$A_i(\mathbf{x}) = G_{ik}(\mathbf{x}, \mathbf{x}_0), \quad B_i(\mathbf{x}) = \gamma(\mathbf{x}) n_i(\mathbf{x}), \tag{3.3}$$

where the singular point $\mathbf{x}_0$ lies in the exterior of D, and k is a free index defining the orientation of the point force. With these choices, identity (A.4) yields

$$\int_D \frac{\partial}{\partial x_j}[G_{ik}(\mathbf{x}, \mathbf{x}_0)\gamma(\mathbf{x})n_j(\mathbf{x})]n_i(\mathbf{x})\, dS(\mathbf{x}) = \int_D \frac{\partial}{\partial x_j}[G_{jk}(\mathbf{x}, \mathbf{x}_0)\gamma(\mathbf{x})n_i(\mathbf{x})]n_i(\mathbf{x})\, dS(\mathbf{x}). \tag{3.4}$$

We expand the derivatives of the products on either side, note that the continuity equation requires $\partial G_{jk}(\mathbf{x}, \mathbf{x}_0)/\partial x_j = 0$, take into consideration the unit-length constraints $|\mathbf{n}| = 1$ and $(\nabla \mathbf{n}) \cdot \mathbf{n} = \frac{1}{2}\nabla|\mathbf{n}|^2 = 0$, and thus find

$$\begin{aligned} &\int_D \frac{\partial \gamma}{\partial x_j} G_{ik}(\mathbf{x}, \mathbf{x}_0) n_j(\mathbf{x}) n_i(\mathbf{x})\, dS(\mathbf{x}) + \int_D \gamma(\mathbf{x}) \frac{\partial G_{ik}(\mathbf{x}, \mathbf{x}_0)}{\partial x_j} n_j(\mathbf{x}) n_i(\mathbf{x})\, dS(\mathbf{x}) \\ &\quad + \int_D \gamma(\mathbf{x}) G_{ik}(\mathbf{x}, \mathbf{x}_0) \frac{\partial n_j}{\partial x_j} n_j(\mathbf{x})\, dS(\mathbf{x}) = \int_D \frac{\partial \gamma}{\partial x_j} G_{jk}(\mathbf{x}, \mathbf{x}_0)\, dS(\mathbf{x}). \end{aligned} \tag{3.5}$$

Straightforward rearrangement of (3.5) yields

$$\begin{aligned} &\int_D G_{ik}(\mathbf{x}, \mathbf{x}_0) \left[\gamma \frac{\partial n_j}{\partial x_j} n_i - \frac{\partial \gamma}{\partial x_j}(\delta_{ij} - n_j n_i) \right](\mathbf{x})\, dS(\mathbf{x}) \\ &\quad = -\int_D \gamma(\mathbf{x}) \frac{\partial G_{ik}(\mathbf{x}, \mathbf{x}_0)}{\partial x_j} n_j(\mathbf{x}) n_i(\mathbf{x})\, dS(\mathbf{x}). \end{aligned} \tag{3.6}$$

The left-hand hand side of (3.6) is the kth component of the single-layer potential with jump in traction given by (3.2).

In summary, we have expressed the single-layer potential associated with (3.2), to be denoted by $\mathbf{I}^S$, in terms of an interfacial distribution of point-force dipoles in the form

$$I_j^S(\mathbf{x}_0) = \int_D G_{ij}(\mathbf{x}, \mathbf{x}_0) \Delta f_i(\mathbf{x})\, dS(\mathbf{x}) = -\int_D \gamma(\mathbf{x}) \frac{\partial G_{ij}(\mathbf{x}, \mathbf{x}_0)}{\partial x_k} n_i(\mathbf{x}) n_k(\mathbf{x})\, dS(\mathbf{x}). \tag{3.7}$$

To be more specific, we consider the free-space point-force dipole given by

$$\frac{\partial G_{ij}(\mathbf{x}, \mathbf{x}_0)}{\partial x_k} = \frac{\delta_{ij}\hat{x}_k - \delta_{ik}\hat{x}_j - \delta_{jk}\hat{x}_i}{|\hat{\mathbf{x}}|^3} + 3\frac{\hat{x}_i \hat{x}_j \hat{x}_k}{|\hat{\mathbf{x}}|^5}, \tag{3.8}$$

where $\hat{\mathbf{x}} = \mathbf{x} - \mathbf{x}_0$ (e.g., Pozrikidis [133, p. 261]). Substituting this expression into the last integral of (3.7), we find

$$I_j^S(\mathbf{x}_0) = \int_D \gamma(\mathbf{x}) \frac{\hat{x}_j}{|\hat{\mathbf{x}}|^3} \left[1 - 3\frac{[\hat{\mathbf{x}} \cdot \mathbf{n}(\mathbf{x})]^2}{|\hat{\mathbf{x}}|^2} \right] dS(\mathbf{x}), \tag{3.9}$$

which is consistent with an expression for interfaces with constant surface tension presented by Zinchenko *et al.* [210, Eq. (40)], working in surface curvilinear coordinates. Zinchenko

et al. [211] find that, with proper regularizaton, as will be discussed in later sections, the so-called "curvatureless" formulation expressed by (3.9) has certain computational advantages over the primary single-layer formulation for shapes with strongly varying mean curvature.

Now, because the tensor **nn** is symmetric, the Green's function dipole on the right-hand side of (3.7) may be replaced by its symmetric component with respect to the repeated indices i and k. Invoking the definition of the Green's function stress tensor, $T_{ijk} = -\delta_{ik} p_j + \partial G_{ij}/\partial x_k + \partial G_{kj}/\partial x_i$, where p_j is the Green's function vector for the pressure (e.g., Pozrikidis [127, p. 25]), we write

$$I_j^{\mathrm{S}}(\mathbf{x}_0) = -\frac{1}{2}\int_D \gamma(\mathbf{x})\, p_j(\mathbf{x}, \mathbf{x}_0)\, dS(\mathbf{x}) - \frac{1}{2}\int_D \gamma(\mathbf{x}) T_{ijk}(\mathbf{x}, \mathbf{x}_0) n_i(\mathbf{x}) n_k(\mathbf{x})\, dS(\mathbf{x}). \quad (3.10)$$

If the flow is not enclosed entirely by an impenetrable boundary, the first term on the right-hand side of (3.10) expresses the velocity at the point $\mathbf{x}_0$ due to a distribution of point sources with uniform density proportional to the surface tension (Pozrikidis [127, p. 80]). For example, in the case of flow in an infinite domain, $p_j(\mathbf{x}, \mathbf{x}_0) = 2\hat{x}_j/|\hat{\mathbf{x}}|^3$. The second integral on the right-hand side of (3.10) is the double-layer potential with vectorial strength proportional to the normal vector. As the point $\mathbf{x}_0$ crosses the interface, each one of the integrals on the right-hand side of (3.10) suffers a discontinuity, but the two discontinuities cancel one another to give a net contribution that is continuous throughout the domain of flow.

When the point $\mathbf{x}_0$ lies at the interface, the integrand of the double-layer potential in (3.10) is nonsingular: as the integration point $\mathbf{x}$ approaches the evaluation point $\mathbf{x}_0$, the stress tensor T_{ijk} behaves like the one corresponding to the free-space Green's function, $T_{ijk}(\mathbf{x}, \mathbf{x}_0) \simeq -6\hat{x}_i \hat{x}_j \hat{x}_k/|\hat{\mathbf{x}}|^5$, the distance $\hat{\mathbf{x}}$ tends to become orthogonal to the normal vector $\mathbf{n}$, the projection $\hat{\mathbf{x}} \cdot \mathbf{n}$ vanishes quadratically with respect to $\hat{\mathbf{x}}$, and the kernel of the double-layer potential tends to a finite value that depends on the orientation of $\hat{\mathbf{x}}$. In contrast, the integrand of the first integral on the left-hand side of (3.10) diverges quadratically with respect to $|\hat{\mathbf{x}}|$.

Restricting our attention to neutrally buoyant particles, we substitute expression (3.10) into the boundary-integral representation (2.6) and obtain a representation in terms of a Laplace single-layer potential and a Stokes double-layer potential,

$$u_j(\mathbf{x}_0) = u_j^{\infty}(\mathbf{x}_0) + \frac{1}{16\pi\mu_s}\sum_{m=1}^{N}\int_{D_m} \gamma(\mathbf{x})\, p_j(\mathbf{x}, \mathbf{x}_0)\, dS(\mathbf{x}) + \frac{1}{8\pi\mu_s}\sum_{m=1}^{N}\int_{D_m}\left[\frac{1}{2}\gamma n_i + \mu_s(1-\lambda_m)u_i\right](\mathbf{x}) T_{ijk}(\mathbf{x}, \mathbf{x}_0) n_k(\mathbf{x})\, dS(\mathbf{x}). \quad (3.11)$$

The representation (3.11) is valid at a point $\mathbf{x}_0$ that lies in the exterior of a particle. For a point that lies in the interior of the qth interface, all terms on the right-hand side should be divided by the viscosity ratio λ_q. Taking the limit as the point $\mathbf{x}_0$ approaches the qth interface, we obtain the integral equation

$$u_j(\mathbf{x}_0) = \frac{2}{1+\lambda_q}\left[u_j^{\infty}(\mathbf{x}_0) + \frac{1}{16\pi\mu_s}\sum_{m=1}^{N}\int_{D_m}^{\mathrm{PV}} \gamma(\mathbf{x})\, p_j(\mathbf{x}, \mathbf{x}_0)\, dS(\mathbf{x})\right] + \frac{1}{8\pi\mu_s}\sum_{m=1}^{N}\int_{D_m}^{\mathrm{PV}}\left[\frac{1}{2}\gamma n_i + \mu_s(1-\lambda_m)u_i\right](\mathbf{x}) T_{ijk}(\mathbf{x}, \mathbf{x}_0) n_k(\mathbf{x})\, dS(\mathbf{x}), \quad (3.12)$$

where PV denotes the principal value of the underlying integral. The computation of the principal value of the integrals on the right-hand side of (3.12) will be discussed in Section 8.

3.3. *Suspension Rheology*

Carrying out the multipole expansion, we find that the coefficient of the stresslet deduced from the double-layer integral on the right-hand side of (3.11) is given by

$$\Sigma_{ik} = c\delta_{ik} - \sum_{m=1}^{N} \int_{D_m} [\gamma n_i n_k + \mu_s(1-\lambda_m)(u_i n_k + u_k n_i)](\mathbf{x})\, dS(\mathbf{x}), \qquad (3.13)$$

where c is an arbitrary constant (e.g., Pozrikidis [127, pp. 47, 143]). Batchelor [12] showed that the right-hand side of (3.13) represents the contribution of the interfaces to the effective stress tensor of a suspension. Straightforward rearrangement of (3.13) yields

$$\Sigma_{ik} = c'\delta_{ik} + 2W_{ik} - \mu_s \sum_{m=1}^{N} (1-\lambda_m) \int_{D_m} (u_i n_k + u_k n_i)](\mathbf{x})\, dS(\mathbf{x}), \qquad (3.14)$$

where c' is a new constant, and

$$W_{ik} = \frac{1}{2} \sum_{m=1}^{N} \int_{D_m} \gamma(\mathbf{x})[\delta_{ik} - n_i(\mathbf{x}) n_k(\mathbf{x})]\, dS(\mathbf{x}) \qquad (3.15)$$

is the surface energy tensor generalized for varying surface tension [156]. When the surface tension γ is constant, the trace of $\mathbf{W}$ is equal to γS_D, where S_D is the surface area of the interfaces. The significant new result is that the right-hand side of (3.14) may be evaluated from knowledge of the shape of the interfaces and interfacial distributions of the velocity and surface tension; when $\lambda_m = 1$, for all m, the interfacial velocity is not required.

Applying identity (A.5) of the Appendix with $B_j = \gamma n_j x_l$, where l is a free index, we find

$$W_{ik} = \frac{1}{2} \sum_{m=1}^{N} \int_{D_m} x_i \Delta f_k(\mathbf{x})\, dS(\mathbf{x}), \qquad (3.16)$$

where $\Delta\mathbf{f}$ is given by (3.2). Substituting this expression into (3.14), we recover the general form

$$\Sigma_{ik} = c'\delta_{ik} + \sum_{m=1}^{N} \int_{D_m} [x_i \Delta f_k - \mu_s(1-\lambda_m)(u_i n_k + u_k n_i)](\mathbf{x})\, dS(\mathbf{x}), \qquad (3.17)$$

which is applicable for an arbitrary traction discontinuity $\Delta\mathbf{f}$.

3.4. *Evolution of the Concentration of an Immiscible Surfactant*

When an interface is occupied by an insoluble surfactant, the evolution of the surfactant concentration must be computed simultaneously with the motion of the interface. In the numerical implementation, the interface is regarded either as a material surface or as a

surface of discontinuity consisting of a continuous distribution of point particles or marker points that are labeled permanently by two convected surface curvilinear coordinates (ξ, η).

Kinematic considerations require that the normal component of the marker-point velocity be equal to the normal component of the velocity of the fluid, but the tangential component may be arbitrary. The general form of the marker-point velocity is

$$\mathbf{U} = (\mathbf{u} \cdot \mathbf{n})\mathbf{n} + \mathbf{w}, \tag{3.18}$$

where $\mathbf{u}$ is the velocity of the fluid, and $\mathbf{w}$ is an arbitrary tangential velocity. When $\mathbf{w} = \mathbf{0}$, the marker points move with the fluid velocity normal to the interface, whereas when $\mathbf{w} = \mathbf{P} \cdot \mathbf{u}$, the marker points move with the whole of the fluid velocity.

The evolution of the concentration of an *immiscible* surfactant that diffuses over the interface but not into the bulk of the fluids is governed by the equation

$$\left(\frac{\partial \Gamma}{\partial t}\right)_{\xi,\eta} = \mathbf{w} \cdot \nabla_s \Gamma - \nabla_s \cdot (\Gamma \mathbf{u}_s) - \Gamma 2\kappa_m \mathbf{u} \cdot \mathbf{n} + D_s \nabla_s^2 \Gamma, \tag{3.19}$$

where $\mathbf{u}_s = \mathbf{P} \cdot \mathbf{u}$ is the component of the fluid velocity tangential to the interface, $\nabla_s \equiv \mathbf{P} \cdot \nabla$ is the surface gradient, D_s is the surfactant diffusivity in the plane of the interface, and $\nabla_s^2 \equiv \nabla_s \cdot \nabla_s$ is the surface Laplacian [83, 110, 193, 196, 198]. When $\mathbf{w} = \mathbf{0}$, the first term on the right-hand side of (3.19) does not appear [175]. Expressions for the right-hand side of (3.19) in surface curvilinear coordinates in terms of the contravariant components of the velocity are given by Waxman [193], Zinemanas and Nir [212], Stone and Leal [180], and Wong *et al.* [196]. If the surfactant is miscible into one of both of the bulk phases, an additional flux expressed the net rate of sorption should be included on the right-hand side of (3.19) [110, 61].

To complete the system of governing equations, we require a constitutive equation relating the surface tension γ to the surfactant concentration Γ. In the simplest approximation, physically valid for small surfactant concentrations, we assume the linear law

$$\gamma = \frac{\gamma_0}{1-\beta}\left(1 - \beta\frac{\Gamma}{\Gamma_0}\right), \tag{3.20}$$

where Γ_0 and γ_0 are, respectively, a reference surfactant concentration and the corresponding surface tension. The dimensionless physical constant $\beta = \Gamma_0 RT/\gamma_c$ expresses the sensitivity of the surface tension to the surfactant concentration; R is the ideal gas constant, T is the absolute temperature, and γ_c is the surface tension of a clean interface that is devoid of surfactants (e.g., Adamson [1]). More advanced constitutive equations developed in the context of interfacial thermodynamics are discussed by Pawar and Stebe [118] and Johnson and Borhan [61].

4. INTERFACES WITH ELASTIC PROPERTIES

Clean interfaces and interfaces hosting monolayers of surfactants exhibit isotropic surface tension. Grossly contaminated interfaces, polymerized interfaces, and biological interfaces consisting of lipids and proteins exhibit more involved mechanical properties. Multistructured interfaces, in particular, develop elastic tensions and bending moments similar to those exhibited by thin elastic shells.

For example, the interface between a red blood cell and the ambient plasma consists of a lipid bilayer that is supported by a network of proteins, with an assortment of other proteins also transversing the dual structure [40, 167, 107]. The bilayer is responsible for incompressible behavior that preserves the surface area of any infinitesimal or finite portion of the membrane during deformation. The cytoskeleton is responsible for elastic behavior that causes the cell to return to the resting shape of a biconcave disk in hydrostatics. When a red blood cell is subjected to hydrodynamic stresses, the membrane develops anisotropic elastic tensions and a position-dependent isotropic tension that ensures incompressible deformation. The excess area of a healthy membrane, combined with its low modulus of elasticity, allows the cell to readily deform and squeeze through the microcapillaries.

Membranes of vesicles consisting of lipid bilayers exhibit bending elasticity, that is, resistance to bending from an equilibrium configuration [86]. If the bilayer is symmetric, the equilibrium shape possesses zero mean curvature. More generally, bending elasticity allows vesicles to obtain a great variety of shapes and to exhibit different modes of oscillation in excitation [163].

The mathematical modeling of stresses and bending moments developing over membrane-like interfaces draws heavily from the theory of thin shells [42, 47, 48, 111, 41, 108, 117, 14, 105, 85]. In this theory, the membrane is regarded as a curved two-dimensional medium of small or zero thickness, and its mid-surface is described in parametric form in terms of two-surface curvilinear coordinates. Three approaches are available for describing the membrane deformation, for deriving equilibrium conditions, and for computing the stresses and moments developing due to deformation. In the first approach, the membrane is regarded as a thin sheet of a three-dimensional material, and asymptotic forms of the governing equations and boundary conditions are derived in the limit of zero thickness (e.g., Le Dret and Raoult [76]). In the second approach, special assumptions are made regarding the deformation of fibers that are normal to the midsurface of the membrane. In the third approach, the third dimension is abandoned at the outset, and the membrane is regarded as a curved two-dimensional medium.

The third approach has significant advantages: It circumvents certain inconsistencies encountered in the first two approaches [20], and it is appropriate for molecular membranes for which the assumption of continuum in the normal direction is not appropriate. Recent work by Steigmann and Ogden [173, 174] and Steigmann [171, 172] has established a rigorous theoretical foundation which allows the consistent computation of the membrane tensions and bending moments from a strain energy function.

4.1. *Stress Resultants and Bending Moments*

Consider a membrane in a specified reference configuration, and label the point particles that compose it by two convected surface curvilinear coordinates (ξ, η), so that a line of constant η, a line of constant ξ, and a line along the unit normal vector $\mathbf{n}^R$ define a system of right-handed but not necessarily orthogonal coordinates, as depicted at the top drawing of Fig. 3. The positions of point particles in the reference state are denoted by $\mathbf{x}^R(\xi, \eta)$. Assume now that the membrane deforms, and denote the new positions of the point particles by $\mathbf{x}(\xi, \eta)$. The developing in-plane stress resultants or elastic tensions $\tau_{\alpha\beta}$, transverse shear tensions q_α, and bending moments $m_{\alpha\beta}$ are illustrated in Fig. 4. In the "membrane approximation" of thin-shell theory, the transverse tensions and bending moments are neglected,

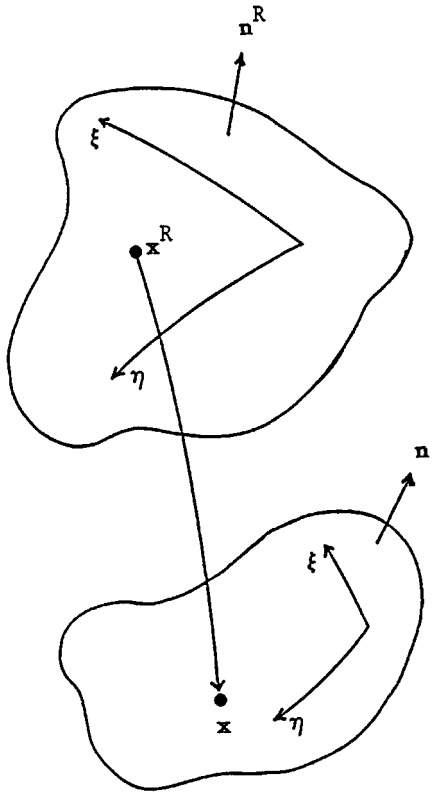

FIG. 3. Schematic illustration of a three-dimensional membrane at the reference and the deformed state. Point particles distributed over the membrane are marked permanently by two convected surface curvilinear coordinates (ξ, η).

and only in-plane stress resultants are considered [24]. This approximation, however, is not appropriate for polymerized capsules and biological membranes where bending moments make an important, if not essential, contribution.

4.2. *Interface Force and Torque Balances in Cartesian Coordinates*

Describing the membrane tensions and bending moments in global Cartesian coordinates facilitates the interfacing of the membrane mechanics to the hydrodynamics on either side of an interface. In the Cartesian formulation, the domain of definition of the membrane tensions and bending moments is extended into the whole three-dimensional space subject to appropriate constraints, as follows [49, 85, 144].

The in-plane tensions are described in terms of the Cartesian tensor τ, so that the in-plane tension exerted on a cross section of the membrane that is normal to the tangential unit vector $\mathbf{b}$ is given by $\mathbf{b} \cdot \tau$ and, furthermore, $\mathbf{n} \cdot \tau = \mathbf{0}$ and $\tau \cdot \mathbf{n} = \mathbf{0}$; the last restriction ensures that the tension lies in the tangential plane. For example, if an interface exhibits isotropic tension γ, $\tau = \gamma \mathbf{P}$, where $\mathbf{P} = \mathbf{I} - \mathbf{nn}$ is the tangential projection operator. The transverse shear tension is described in terms of the Cartesian vector $\mathbf{q}$, so that the transverse shear tension exerted on a cross section of the membrane that is normal to the tangential unit vector $\mathbf{b}$ is given by $\mathbf{b} \cdot \mathbf{q}$ and, furthermore, $\mathbf{n} \cdot \mathbf{q} = 0$. The bending moments are expressed in terms of the Cartesian tensor $\mathbf{m}$, so that the bending moment vector exerted on a cross section

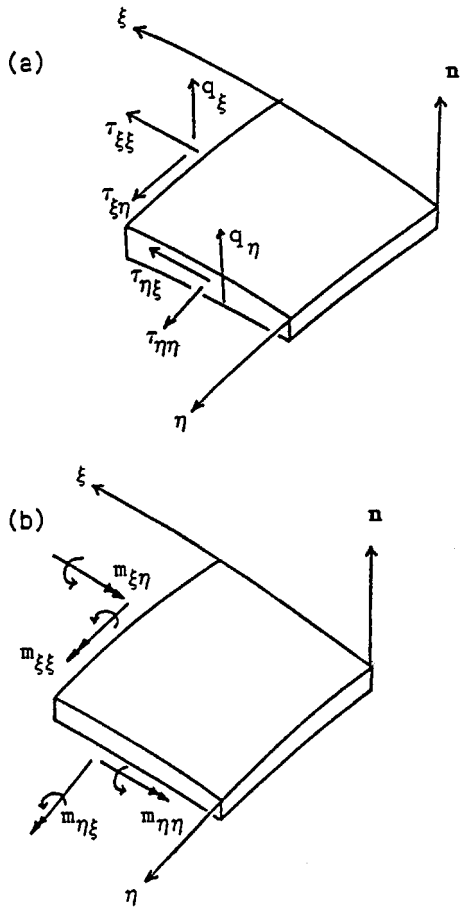

FIG. 4. Depiction of (a) in-plane and transverse shear tensions (stress resultants), and (b) bending moments developing around the edges of a patch on a three-dimensional membrane.

of the membrane that is normal to the tangential unit vector $\mathbf{b}$ is given by $\mathbf{n} \times (\mathbf{b} \cdot \mathbf{m})$ and, furthermore, $\mathbf{n} \cdot \mathbf{m} = \mathbf{0}$ and $\mathbf{m} \cdot \mathbf{n} = \mathbf{0}$; the last restriction ensures that the moment vector lies in the tangential plane.

Consider a patch of a membrane enclosed by the contour C, as illustrated in Fig. 2. Assuming that the mass and thus the inertia of the membrane is negligible, we perform a force balance over the patch to obtain

$$\int_{\text{patch}} \left(\sigma^{(\text{s})} - \sigma^{(\text{c})}\right) \cdot \mathbf{n}\, dS + \int_C \mathbf{b} \cdot (\tau + \mathbf{qn})\, dl = \mathbf{0}, \tag{4.1}$$

where $\mathbf{t}$ is the unit vector tangential to C, $\mathbf{b} = \mathbf{t} \times \mathbf{n}$ is the unit vector that is tangential to the membrane and lies in a plane that is normal to the contour C, and l is the arc length along C. Using the divergence theorem to convert the contour integral into a surface integral on the right-hand side of (4.1), and taking the limit as the size of the patch becomes infinitesimal, we find that the jump in the hydrodynamic traction across the membrane is given by

$$\Delta\mathbf{f} \equiv \left(\sigma^{(\text{s})} - \sigma^{(\text{c})}\right) \cdot \mathbf{n} = -(\mathbf{P} \cdot \nabla) \cdot (\tau + \mathbf{qn}) = -\text{Trace}[(\mathbf{P} \cdot \nabla)(\tau + \mathbf{qn})], \tag{4.2}$$

(e.g., Pozrikidis [144]). The right-hand side of (4.2) expresses the surface divergence of the

generalized elastic tension tensor in Cartesian coordinates [110]. The tangential derivatives are taken with respect to two isometric orthogonal rectilinear coordinates that are tangential to the membrane at the point where the divergence is evaluated.

An analogous torque balance with respect to the arbitrary point $\mathbf{x}_c$ requires

$$\int_{\text{patch}} (\mathbf{x}-\mathbf{x}_c)\times\left[\left(\sigma^{(\text{s})}-\sigma^{(\text{c})}\right)\cdot\mathbf{n}\right]dS+\int_C(\mathbf{x}-\mathbf{x}_c)\times[\mathbf{b}\cdot(\tau+\mathbf{qn})]\,dl + \int_C \mathbf{n}\times(\mathbf{b}\cdot\mathbf{m})\,dl=\mathbf{0}. \tag{4.3}$$

Using the divergence theorem to convert the contour integral into a surface integral on the right-hand side of (4.3), taking the limit as the size of the patch becomes infinitesimal, and then using the force balance (4.2), we derive an expression for the transverse shear tension,

$$\mathbf{q}=[(\mathbf{P}\cdot\nabla)\cdot\mathbf{m}]\cdot\mathbf{P}=\text{Trace}[(\mathbf{P}\cdot\nabla)\mathbf{m}]\cdot\mathbf{P}, \tag{4.4}$$

and another expression for the antisymmetric part of the in-plane tension tensor,

$$\tau-\tau^T=\mathbf{B}\cdot\mathbf{m}-\mathbf{m}^T\cdot\mathbf{B}, \tag{4.5}$$

where the superscript T denotes the matrix transpose, and $\mathbf{B}=\nabla\mathbf{n}$ is the symmetric Cartesian curvature tensor (e.g., [19, 193, 144]).

4.3. *Interface Force and Torque Balances in Surface Curvilinear Coordinates*

The Cartesian formulation described in Section 4.2 requires that the membrane tensions and bending moments be extended into the whole space in an appropriate fashion. This extension can be avoided by working in surface curvilinear coordinates (e.g., Barthès-Biesel [8]). To set up this formulation, we introduce the generally nonunit tangential vectors

$$\mathbf{t}_\xi\equiv\frac{\partial\mathbf{x}}{\partial\xi},\quad \mathbf{t}_\eta\equiv\frac{\partial\mathbf{x}}{\partial\eta} \tag{4.6}$$

and the corresponding arc length metric coefficients

$$h_\xi=|\mathbf{t}_\xi|,\quad h_\eta=|\mathbf{t}_\eta|. \tag{4.7}$$

The *first fundamental form* of the surface is defined as the square of the length of an infinitesimal fiber whose end-points are separated by a vector corresponding to the infinitesimal coordinates $d\xi$ and $d\eta$,

$$(dl)^2=a_{\xi\xi}(d\xi)^2+2a_{\xi\eta}\,d\xi\,d\eta+a_{\eta\eta}(d\eta)^2, \tag{4.8}$$

where

$$a_{\xi\xi}=h_\xi^2,\quad a_{\xi\eta}=a_{\eta\xi}=\mathbf{t}_\xi\cdot\mathbf{t}_\eta,\quad a_{\eta\eta}=h_\eta^2. \tag{4.9}$$

The surface area of a patch confined between two ξ or η segments with infinitesimal spans $d\xi$ and $d\eta$ is equal to $dS=\sqrt{a}d\xi d\eta$, where $a=h_\xi^2h_\eta^2-a_{\xi\eta}^2$.

The *second fundamental form* of the surface is defined as the quadratic form

$$Q = -b_{\xi\xi}(d\xi)^2 - 2b_{\xi\eta}\, d\xi\, d\eta - b_{\eta\eta}(d\eta)^2, \tag{4.10}$$

where

$$b_{\xi\xi} = \mathbf{n} \cdot \frac{\partial \mathbf{t}_\xi}{\partial \xi}, \quad b_{\xi\eta} = b_{\eta\xi} = \mathbf{n} \cdot \frac{\partial \mathbf{t}_\xi}{\partial \eta} = \mathbf{n} \cdot \frac{\partial \mathbf{t}_\eta}{\partial \xi}, \quad b_{\eta\eta} = \mathbf{n} \cdot \frac{\partial \mathbf{t}_\eta}{\partial \eta}, \tag{4.11}$$

$\mathbf{n} = \mathbf{t}_\xi \times \mathbf{t}_\eta / |\mathbf{t}_\xi \times \mathbf{t}_\eta|$ is the unit normal vector, and $b_{\alpha\beta}$ is the symmetric surface curvature tensor. The normal curvature of the surface in the direction of an infinitesimal vector whose end-points correspond to the infinitesimal increments $d\xi$ and $d\eta$ is equal to the ratio of the second to the first fundamental form of the surface.

Next, we introduce the surface contravariant components of the tension tensor τ denoted by $\tau^{\alpha\beta}$, the surface contravariant components of the transverse shear tension vector denoted by q^ξ and q^η, and the surface contravariant components of the bending moment tensor $\mathbf{m}$ denoted by $m^{\alpha\beta}$. Greek superscripts and subscripts stand for ξ or η. Subject to these definitions, the force equilibrium Eq. (4.2) takes the form

$$\Delta \mathbf{f} \equiv \left(\sigma^{(\mathrm{s})} - \sigma^{(\mathrm{c})}\right) \cdot \mathbf{n} = \Delta f^n \mathbf{n} + \Delta f^\xi \mathbf{t}_\xi + \Delta f^\eta \mathbf{t}_\eta, \tag{4.12}$$

where

$$\Delta f^n = -b_{\alpha\beta}\tau^{\alpha\beta} - q^\beta|_\beta, \quad \Delta f^\xi = -\tau^{\beta\xi}|_\beta + b^\xi_\alpha q^\alpha, \quad \Delta f^\eta = -\tau^{\beta\eta}|_\beta + b^\eta_\alpha q^\alpha, \tag{4.13}$$

[108, p. 165; 193, Eq. (3.5)]. Correspondingly, the torque equilibrium Eqs. (4.4) and (4.5) take the form

$$q^\xi = m^{\alpha\xi}|_\alpha, \quad q^\eta = m^{\alpha\eta}|_\alpha, \quad \tau^{\xi\eta} - \tau^{\eta\xi} = b^\xi_\alpha m^{\alpha\eta} - b^\eta_\alpha m^{\alpha\xi} \tag{4.14}$$

where the mixed components b^β_α are related to the pure components $b_{\alpha\beta}$ by the relation $b_{\beta\alpha} = a_{\beta\gamma} b^\gamma_\alpha$ (Møllmann [108, p. 165]; Waxman [193, Eq. (3.9)]. A vertical bar signifies the covariant derivative with respect to the subscribed variable defined in terms of the Christoffel symbols [5].

4.4. *Interface Force and Torque Balance in Lines of Principal Curvatures*

Considerable simplifications occur by referring to surface curvilinear coordinates whose tangential vector at every point is oriented in the direction of the principal curvatures, defined as the *lines of principal curvature*. A line of constant η, a line of constant ξ, and a line directed along the unit normal vector $\mathbf{n}$ define a right-handed system of orthogonal curvilinear coordinates. The directions of the stress resultants and bending moments are defined in Fig. 4. In the case of an axisymmetric interface supporting axisymmetric tensions, to be discussed in Section 5, the lines of principal curvatures are and remain the traces of the membrane in meridional and azimuthal planes.

In surface curvilinear coordinates that are lines of principal curvatures, the decomposition (4.12) takes the preferred form

$$\Delta \mathbf{f} \equiv \left(\sigma^{(\mathrm{s})} - \sigma^{(\mathrm{c})}\right) \cdot \mathbf{n} = \Delta f^n \mathbf{n} + \Delta f'^\xi \mathbf{e}_\xi + \Delta f'^\eta \mathbf{e}_\eta, \tag{4.15}$$

where $\mathbf{n}$ is the unit normal vector pointing into the ambient fluid and $\mathbf{e}_\xi \equiv \mathbf{t}_\xi / |\mathbf{t}_\xi|$, $\mathbf{e}_\eta \equiv$

$\mathbf{t}_\eta/|\mathbf{t}_\eta|$ are unit tangential vectors. The normal and tangential components of the traction discontinuity are given by

$$\Delta f^n = \kappa_\xi \tau_{\xi\xi} + \kappa_\eta \tau_{\eta\eta} - \frac{1}{h_\xi h_\eta}\left[\frac{\partial}{\partial\xi}(h_\eta q_\xi) + \frac{\partial}{\partial\eta}(h_\xi q_\eta)\right], \tag{4.16}$$

$$\Delta f'^{\xi} = -\frac{1}{h_\xi h_\eta}\left[\frac{\partial}{\partial\xi}(h_\eta \tau_{\xi\xi}) + \frac{\partial}{\partial\eta}(h_\xi \tau_{\eta\xi}) + \frac{\partial h_\xi}{\partial\eta}\tau_{\xi\eta} - \frac{\partial h_\eta}{\partial\xi}\tau_{\eta\eta}\right] - \kappa_\xi q_\xi, \tag{4.17}$$

$$\Delta f'^{\eta} = -\frac{1}{h_\xi h_\eta}\left[\frac{\partial}{\partial\xi}(h_\eta \tau_{\xi\eta}) + \frac{\partial}{\partial\eta}(h_\xi \tau_{\eta\eta}) - \frac{\partial h_\xi}{\partial\eta}\tau_{\xi\xi} + \frac{\partial h_\eta}{\partial\xi}\tau_{\eta\xi}\right] - \kappa_\eta q_\eta, \tag{4.18}$$

where $\kappa_\xi = -b_{\xi\xi}/h_\xi^2$ and $\kappa_\eta = -b_{\eta\eta}/h_\eta^2$ are the principal curvatures. Moreoever, expressions (4.14) simplify to

$$q_\xi = \frac{1}{h_\xi h_\eta}\left[\frac{\partial}{\partial\xi}(h_\eta m_{\xi\xi}) + \frac{\partial}{\partial\eta}(h_\xi m_{\eta\xi}) + \frac{\partial h_\xi}{\partial\eta}m_{\xi\eta} - \frac{\partial h_\eta}{\partial\xi}m_{\eta\eta}\right], \tag{4.19}$$

$$q_\eta = \frac{1}{h_\xi h_\eta}\left[\frac{\partial}{\partial\xi}(h_\eta m_{\xi\eta}) + \frac{\partial}{\partial\eta}(h_\xi m_{\eta\eta}) - \frac{\partial h_\xi}{\partial\eta}m_{\xi\xi} + \frac{\partial h_\eta}{\partial\xi}m_{\eta\xi}\right], \tag{4.20}$$

$$\tau_{\xi\eta} - \tau_{\eta\xi} = -\kappa_\xi m_{\xi\eta} + \kappa_\eta m_{\eta\xi}, \tag{4.21}$$

(e.g., Møllmann [108, p. 33]). In Section 5, we shall present the specific forms of these expressions for axisymmetric membranes in cylindrical polar coordinates.

4.5. *Surface Deformation*

As a prelude to evaluating the elastic tensions, we refer to Fig. 3 and introduce the three-dimensional Cartesian relative deformation gradient tensor $\mathbf{F}$ with components

$$F_{ij} = \left(\frac{\partial x_i}{\partial x_j^{\mathrm{R}}}\right)_{\xi,\eta}. \tag{4.22}$$

Let the infinitesimal vector $d\mathbf{l}^{\mathrm{R}}$ describe a small fiber that is either tangential or normal to the membrane at the reference state. After deformation, the fiber has rotated and stretched or compressed to its image described by

$$d\mathbf{l} = \mathbf{F}\cdot d\mathbf{l}^{\mathrm{R}}. \tag{4.23}$$

The nine components of the relative deformation gradient tensor $\mathbf{F}$ may be evaluated from knowledge of the images of two fibers that are tangential to the membrane at a point, and the image of a fiber that is normal to the membrane at that point. In the present formulation, the image of a fiber that is normal to the membrane is assumed to vanish, so that the deformation of this fiber does not enter the computation of the elastic tensions explicitly, but only implicitly by means of the deformation of the tangential fibers, and according to constitutive laws expressing membrane material properties.

For the purpose of computing the elastic tensions, Eq. (4.23) is replaced by the equation

$$d\mathbf{l} = \mathbf{F}^{\mathrm{S}}\cdot d\mathbf{l}^{\mathrm{R}}, \tag{4.24}$$

where

$$\mathbf{F}^{\mathrm{S}} \equiv \mathbf{F} \cdot (\mathbf{I} - \mathbf{n}^{\mathrm{R}}\mathbf{n}^{\mathrm{R}}) \tag{4.25}$$

is the relative *surface* deformation gradient, and the superscript S stands for "surface." Clearly, $\mathbf{n}^{\mathrm{R}}$ is an eigenvector of $\mathbf{F}^{\mathrm{S}}$ corresponding to a vanishing eigenvalue, which shows that $\mathbf{F}^{\mathrm{S}}$ is singular.

If $d\mathbf{l}^{\mathrm{R}}$ is a tangential fiber at the reference state, then $d\mathbf{l}$ is also a tangential fiber in the deformed state, and this requires $\mathbf{n} \cdot d\mathbf{l} = \mathbf{n} \cdot \mathbf{F}^{\mathrm{S}} \cdot d\mathbf{l}^{\mathrm{R}} = 0$. Since, however, the orientation of $d\mathbf{l}^{\mathrm{R}}$ is arbitrary, it must be that $\mathbf{n} \cdot \mathbf{F}^{\mathrm{S}} = \mathbf{0}$, which suggests that $\mathbf{F}^{\mathrm{S}} = (\mathbf{I} - \mathbf{nn}) \cdot \mathbf{F}^{\mathrm{S}}$ or

$$\mathbf{F}^{\mathrm{S}} \equiv (\mathbf{I} - \mathbf{nn}) \cdot \mathbf{F} \cdot (\mathbf{I} - \mathbf{n}^{\mathrm{R}}\mathbf{n}^{\mathrm{R}}). \tag{4.26}$$

Thus, $\mathbf{n}$ is an eigenvector of the transpose of $\mathbf{F}^{\mathrm{S}}$ corresponding to the vanishing eigenvalue. The polar decomposition theorem allows us to write $\mathbf{F}^{\mathrm{S}} = \mathbf{R} \cdot \mathbf{U} = \mathbf{V} \cdot \mathbf{R}$, where $\mathbf{R}$ is an orthogonal matrix expressing plane rotation, and $\mathbf{U}$ and $\mathbf{V}$ are the positive-definite and symmetric right or left stretch tensors expressing pure deformation.

Following standard procedure in the theory of elasticity (e.g., [14, 47, 48]), we introduce the positive-definite and symmetric surface left Cauchy–Green deformation tensor

$$\mathbf{V}^2 \equiv \mathbf{F}^{\mathrm{S}} \cdot \mathbf{F}^{\mathrm{S}^T}, \tag{4.27}$$

where the superscript T denotes the matrix transpose. The eigenvalues of $\mathbf{V}^2$ are equal to λ_1^2, λ_2^2, and 0, corresponding to the orthogonal tangential eigenvectors $\mathbf{v}_1$, $\mathbf{v}_2$, and to the normal vector $\mathbf{n}$. The eigenvectors of $\mathbf{V}^2$ are also eigenvectors of the tension tensor τ.

In terms of the principal elastic tensions τ_1^{P} and τ_2^{P} and the unit tangential eigenvectors $\mathbf{e}_1 = \mathbf{v}_1/|\mathbf{v}_1|$ and $\mathbf{e}_2 = \mathbf{v}_2/|\mathbf{v}_2|$, the part of the symmetric tension tensor is given by the spectral decomposition

$$\tau = \tau_1^{\mathrm{P}}\mathbf{e}_1\mathbf{e}_1 + \tau_2^{\mathrm{P}}\mathbf{e}_2\mathbf{e}_2. \tag{4.28}$$

In the presence of bending moments, the tension tensor has an additional antisymmetric component, as will be discussed later in this section.

4.6. *Constitutive Equations for the Elastic Tensions*

Next, we proceed to relate the tensions to the surface strains by means of a constitutive equation. As a prelude, we consider a three-dimensional elastic medium and express the force exerted on a small material patch of surface area dS that is perpendicular to the unit normal vector $\mathbf{n}$ in terms of the Eulerian stress tensor σ, in the familiar form

$$d\mathbf{f} = \mathbf{n} \cdot \sigma \, dS. \tag{4.29}$$

Furthermore, we introduce the *first Piola–Kirchhoff tensor* $\mathbf{T}$, also called the *Lagrange or nominal stress tensor,* and the *Piola–Kirchhoff tensor* $\mathbf{S}$, defined by the relations

$$d\mathbf{f} = \mathbf{n} \cdot \sigma \, dS = \mathbf{n}^{\mathrm{R}} \cdot \mathbf{T} \, dS^{\mathrm{R}} = \mathbf{n}^{\mathrm{R}} \cdot \mathbf{S} \cdot \mathbf{F}^T \, dS^{\mathrm{R}}, \tag{4.30}$$

where $\mathbf{n}^{\mathrm{R}}$ is the unit vector normal to the patch at a reference state, dS^{R} is the corresponding

surface area, and the superscript T denotes the matrix transpose (e.g., [42, p. 438; 117, p. 152]). The Eulerian stress tensor σ is related to the first Piola–Kirchhoff tensor $\mathbf{T}$ and to the Piola–Kirchhoff tensor $\mathbf{S}$ by the equation

$$\sigma = \frac{1}{J}\mathbf{F}\cdot\mathbf{T} = \frac{1}{J}\mathbf{F}\cdot\mathbf{S}\cdot\mathbf{F}^T, \tag{4.31}$$

where $J = \mathrm{Det}(\mathbf{F})$ is the fractional volume of an infinitesimal volume element after the deformation; for an incompresible material, $J = 1$. For a Green-elastic or hyperelastic three-dimensional medium, the first Piola–Kirchhoff tensor and the Piola–Kirchhoff tensor derive from a strain-energy function $W(\mathbf{F})$ by means of the relations

$$T_{ij} = \frac{\partial W}{\partial F_{ij}}, \quad S_{ij} = \frac{\partial W}{\partial E_{ij}}, \tag{4.32}$$

where $\mathbf{E} = \frac{1}{2}(\mathbf{F}^T\cdot\mathbf{F} - \mathbf{I})$ is the Green (material or Lagrangean) strain tensor (e.g., [14; 42, p. 449; 47, p. 7; 117, pp. 204–209]).

Considering now the two-dimensional analog of the preceding equations over the curved surface of a membrane in the absence of bending moments, we replace Eq. (4.31) by

$$\tau = \frac{1}{J^{\mathrm{S}}}\mathbf{F}^{\mathrm{S}}\cdot\mathbf{T}^{\mathrm{S}} = \frac{1}{J^{\mathrm{S}}}\mathbf{F}^{\mathrm{S}}\cdot\mathbf{S}^{\mathrm{S}}\cdot\mathbf{F}^{\mathrm{S}^T}, \tag{4.33}$$

where $J^{\mathrm{S}} = \lambda_1\lambda_2$ is the fractional surface area of a material membrane patch after deformation, and $\mathbf{T}^{\mathrm{S}}$ and $\mathbf{S}^{\mathrm{S}}$ are the surface Piola–Kirchhoff tensors. The counterparts of relations (4.32) are

$$T^{\mathrm{S}}_{ij} = \frac{\partial W^{\mathrm{S}}}{\partial F^{\mathrm{S}}_{ij}}, \quad S^{\mathrm{S}}_{ij} = \frac{\partial W^{\mathrm{S}}}{\partial E^{\mathrm{S}}_{ij}}, \tag{4.34}$$

where $\mathbf{E}^{\mathrm{S}} = \frac{1}{2}(\mathbf{F}^{\mathrm{S}^T}\cdot\mathbf{F}^{\mathrm{S}} - \mathbf{I})$ is the surface Green (material or Lagrangian) strain tensor.

Referring to local Cartesian coordinates with two axes parallel to the principal directions of the tension tensor at a point, and using Eqs. (4.33) and (4.34), we find that the principal tensions are given by

$$\tau^{\mathrm{P}}_1 = \frac{1}{\lambda_2}\frac{\partial W^{\mathrm{S}}}{\partial\lambda_1}, \quad \tau^{\mathrm{P}}_2 = \frac{1}{\lambda_1}\frac{\partial W^{\mathrm{S}}}{\partial\lambda_2}. \tag{4.35}$$

Expression (4.28) combined with Eqs. (4.35) provides us with a complete description of the elastic tensions.

Kinematic constraints require that the surface strain-energy function W^{S} depend on the surface deformation gradient only through strain invariants. Skalak *et al.* [168] introduced the invariants

$$I^{\mathrm{S}}_1 \equiv \lambda_1^2 + \lambda_2^2 - 2, \quad I^{\mathrm{S}}_2 \equiv \lambda_1^2\lambda_2^2 - 1, \tag{4.36}$$

in terms of which expressions (4.35) take the form

$$\tau^{\mathrm{P}}_1 = 2\frac{\lambda_1}{\lambda_2}\frac{\partial W^{\mathrm{S}}}{\partial I^{\mathrm{S}}_1} + 2\lambda_1\lambda_2\frac{\partial W^{\mathrm{S}}}{\partial I^{\mathrm{S}}_2}, \quad \tau^{\mathrm{P}}_2 = 2\frac{\lambda_2}{\lambda_1}\frac{\partial W^{\mathrm{S}}}{\partial I^{\mathrm{S}}_1} + 2\lambda_1\lambda_2\frac{\partial W^{\mathrm{S}}}{\partial I^{\mathrm{S}}_2}, \tag{4.37}$$

Substituting expressions (4.37) into (4.28), we find

$$\tau = \frac{2}{\lambda_1\lambda_2}\big(\lambda_1^2\mathbf{e}_1\mathbf{e}_1 + \lambda_2^2\mathbf{e}_2\mathbf{e}_2\big)\frac{\partial W^{\mathrm{S}}}{\partial I_1^{\mathrm{S}}} + 2\lambda_1\lambda_2(\mathbf{e}_1\mathbf{e}_1 + \mathbf{e}_2\mathbf{e}_2)\frac{\partial W^{\mathrm{S}}}{\partial I_2^{\mathrm{S}}}, \tag{4.38}$$

or

$$\tau = \frac{2}{\lambda_1\lambda_2}\frac{\partial W^{\mathrm{S}}}{\partial I_1^{\mathrm{S}}}\mathbf{V}^2 + 2\lambda_1\lambda_2\frac{\partial W^{\mathrm{S}}}{\partial I_2^{\mathrm{S}}}(\mathbf{I} - \mathbf{nn}). \tag{4.39}$$

Note that when $\partial W^{\mathrm{S}}/\partial I_2^{\mathrm{S}} = 0$, the tensions are isotropic.

Skalak *et al.* [168] proposed the following strain energy function for the membrane of a red blood cell,

$$W^{\mathrm{S}} = \frac{B}{4}\left(\frac{1}{2}I_1^{\mathrm{S}^2} + I_1^{\mathrm{S}} - I_2^{\mathrm{S}}\right) + \frac{C}{8}\,I_2^{\mathrm{S}^2}, \tag{4.40}$$

where B and C are physical constants with estimated values on the order of $B = 0.005$ dynes/cm and $C = 100$ dynes/cm. The large magnitude of the constant C compared to the magnitude of B ensures that the membrane is nearly incompressible: a small deviation of I_2^{S} from unity generates large elastic tensions.

Barthès–Biesel and Rallison [11] introduced the alternative strain invariants

$$\Lambda_1 \equiv \ln\lambda_1\lambda_2 = \frac{1}{2}\ln\big(I_2^{\mathrm{S}} + 1\big), \quad \Lambda_2 \equiv \frac{1}{2}\big(\lambda_1^2 + \lambda_2^2\big) - 1 = \frac{1}{2}I_1^{\mathrm{S}}, \tag{4.41}$$

in terms of which expressions (4.35) take the form

$$\tau_1^{\mathrm{P}} = \frac{1}{\lambda_1\lambda_2}\left(\frac{\partial W^{\mathrm{S}}}{\partial\Lambda_1} + \lambda_1^2\frac{\partial W^{\mathrm{S}}}{\partial\Lambda_2}\right), \quad \tau_2^{\mathrm{P}} = \frac{1}{\lambda_1\lambda_2}\left(\frac{\partial W^{\mathrm{S}}}{\partial\Lambda_1} + \lambda_2^2\frac{\partial W^{\mathrm{S}}}{\partial\Lambda_2}\right). \tag{4.42}$$

Substituting expressions (4.42) into (4.28), we find

$$\tau = \frac{1}{\lambda_1\lambda_2}(\mathbf{e}_1\mathbf{e}_1 + \mathbf{e}_2\mathbf{e}_2)\frac{\partial W^{\mathrm{S}}}{\partial\Lambda_1} + \big(\lambda_1^2\mathbf{e}_1\mathbf{e}_1 + \lambda_2^2\mathbf{e}_2\mathbf{e}_2\big)\frac{\partial W^{\mathrm{S}}}{\partial\Lambda_2}, \tag{4.43}$$

or

$$\tau = \frac{1}{\lambda_1\lambda_2}\left[\frac{\partial W^{\mathrm{S}}}{\partial\Lambda_1}(\mathbf{I} - \mathbf{nn}) + \frac{\partial W^{\mathrm{S}}}{\partial\Lambda_2}\mathbf{V}^2\right]. \tag{4.44}$$

Note that when $\partial W^{\mathrm{S}}/\partial\Lambda_2 = 0$, the tensions are isotropic. In the limit of small deformations, the strain energy function obtains the standard Mooney–Rivlin form

$$W^s = \alpha_1\Lambda_1 + \frac{1}{2}(\alpha_1 + \alpha_2)\Lambda_1^2 + \alpha_3(\Lambda_2 - \Lambda_1), \tag{4.45}$$

where α_1, α_2, and α_3 are material constants (see Section 5).

4.7. *Tensions in a Thin Elastic Shell*

It is instructive to compare the results derived in Section 4.6 with corresponding results for the tensions developing in a thin shell of a three-dimensional incompressible elastic material with uniform thickness h (e.g., [47, pp. 156–159; 105, p. 399]). For this purpose, we introduce the *volume* strain invariants

$$I_1^{\mathrm{V}} \equiv \lambda_1^2 + \lambda_2^2 + \frac{1}{\lambda_1^2\lambda_2^2}, \quad I_2^{\mathrm{V}} \equiv \lambda_1^2 + \lambda_2^2 + \lambda_1^2\lambda_2^2, \tag{4.46}$$

and express the principal elastic tensions in terms of the volume strain energy function W^{V} as

$$\begin{aligned} \tau_1^{\mathrm{P}} &= \frac{2h}{\lambda_1\lambda_2}\left(\lambda_1^2 - \frac{1}{\lambda_1^2\lambda_2^2}\right)\left(\frac{\partial W^{\mathrm{V}}}{\partial I_1^{\mathrm{V}}} + \lambda_2^2\frac{\partial W^{\mathrm{V}}}{\partial I_2^{\mathrm{V}}}\right), \\ \tau_2^{\mathrm{P}} &= \frac{2h}{\lambda_1\lambda_2}\left(\lambda_2^2 - \frac{1}{\lambda_1^2\lambda_2^2}\right)\left(\frac{\partial W^{\mathrm{V}}}{\partial I_1^{\mathrm{V}}} + \lambda_1^2\frac{\partial W^{\mathrm{V}}}{\partial I_2^{\mathrm{V}}}\right). \end{aligned} \tag{4.47}$$

The Mooney–Rivlin strain-energy function is given by

$$W^{\mathrm{V}} = \frac{E}{6h}\left[(1-\alpha)\left(I_1^{\mathrm{V}} - 3\right) + \alpha\left(I_2^{\mathrm{V}} - 3\right)\right], \tag{4.48}$$

where E is the volume modulus of elasticity and α is a material parameter varying between 0 and 1; $\alpha = 0$ corresponds to a linear neo-Hookean medium (e.g., Ogden [106, p. 221]). In the limit of small deformations, expression (4.48) reduces to (4.45) with $\alpha_1 = 0, \alpha_2 = \frac{2}{3}E, \alpha_3 = \frac{1}{3}E$, yielding $W^{\mathrm{S}} = \frac{E}{3}(\Lambda_1^2 + \Lambda_2 - \Lambda_1)$, as discussed by Barthès–Biesel and Rallison [11].

4.8. *Constitutive Equations for Bending Moments*

The bending moments developing in a hyperelastic membrane derive from a strain energy function of appropriate strain and bending measures. Nonlinear theories of shells applicable for finite deformations have been developed and reviewed by several authors including Sanders [157], Budiansky and Sanders [20], Budiansky [19], Simmonds and Danielson [166], Naghdi [111], Libai and Simonds [85], and more recently by Steigmann and Ogden [173, 174], and Pozrikidis [144]. Waxman [193] and Steigmann [172] discuss applications in hydrodynamics.

To illustrate the methods, we confine our attention to the most tractable case of infinitesimal displacements, and refer to orthogonal curvilinear coordinates that are lines of principal curvatures (e.g. Møllmann [108, p. 17]). Considering the displacement of a material point particle over the membrane, denoted by $\mathbf{v}$, we introduce the strain measures

$$\begin{aligned} \epsilon_{\xi\xi} &= \frac{1}{h_\xi}\frac{\partial \mathbf{x}}{\partial \xi}\cdot\frac{\partial \mathbf{v}}{\partial \xi}, \quad \epsilon_{\eta\eta} = \frac{1}{h_\eta}\frac{\partial \mathbf{x}}{\partial \eta}\cdot\frac{\partial \mathbf{v}}{\partial \eta}, \\ \epsilon_{\xi\eta} &= \epsilon_{\eta\xi} = \frac{1}{2h_\xi h_\eta}\left(\frac{\partial \mathbf{x}}{\partial \eta}\cdot\frac{\partial \mathbf{v}}{\partial \xi} + \frac{\partial \mathbf{x}}{\partial \xi}\cdot\frac{\partial \mathbf{v}}{\partial \eta}\right). \end{aligned} \tag{4.49}$$

The measure $\epsilon_{\xi\xi}$ expresses the elongation of a fiber in the direction of the ξ axis, the measure $\epsilon_{\eta\eta}$ expresses the elongation of a fiber in the direction of the η axis, and $\epsilon_{\xi\eta}$ is a measure of

the deformation of an infinitesimal patch. Three corresponding measures of bending, $\kappa_{\xi\xi}$, $\kappa_{\eta\eta}$, and $\kappa_{\xi\eta}$ may be defined in terms of the rotation vector ω of a surface patch due to the deformation (e.g., Møllmann [108, pp. 21, 25]). The strain and bending measures may now be used to define the vectorial strain measure

$$\mathbf{h} \equiv (\epsilon_{\xi\xi}, \epsilon_{\xi\eta}, \epsilon_{\eta\eta}, \kappa_{\xi\xi}, \kappa_{\xi\eta}, \kappa_{\eta\eta}), \tag{4.50}$$

and the surface strain energy function

$$W^{\mathrm{S}} = \frac{1}{2}\mathbf{h} \cdot \mathbf{D} \cdot \mathbf{h}, \tag{4.51}$$

where $\mathbf{D}$ is a positive-definite matrix expressing membrane material properties (e.g., Møllmann [108, p. 45]). For example, if the membrane is a thin shell of a three-dimensional isotropic elastic material, the strain energy function may be approximated with *Love's first approximation* describing the infinitesimal displacement of a thin plate of thickness h,

$$\begin{aligned} W^{\mathrm{S}} = {} & \frac{1}{2}\frac{Eh}{1-\nu^2}\left[(1-\nu)\left(\epsilon_{\xi\xi}^2 + 2\epsilon_{\xi\eta}^2 + \epsilon_{\eta\eta}^2\right) + \nu(\epsilon_{\xi\xi} + \epsilon_{\eta\eta})^2\right] \\ & + \frac{E_{\mathrm{B}}}{2}\left[(1-\nu)\left(\kappa_{\xi\xi}^2 + 2\kappa_{\xi\eta}^2 + \kappa_{\eta\eta}^2\right) + \nu(\kappa_{\xi\xi} + \kappa_{\eta\eta})^2\right] \end{aligned} \tag{4.52}$$

where $E_{\mathrm{B}} = Eh^3/[12(1-\nu^2)]$ is the plate modulus of bending, E is the volume modulus of elasticity, and ν is the Poisson ratio (e.g., Fung [42, p. 461]).

In terms of the strain energy function, the stress resultants and bending moments are given by

$$\begin{aligned} \tau_{\xi\xi} &= \frac{\partial W^{\mathrm{S}}}{\partial \epsilon_{\xi\xi}}, \quad \tau_{\xi\eta} = \tau_{\eta\xi} = \frac{1}{2}\frac{\partial W^{\mathrm{S}}}{\partial \epsilon_{\xi\eta}}, \quad \tau_{\eta\eta} = \frac{\partial W^{\mathrm{S}}}{\partial \epsilon_{\eta\eta}}, \\ m_{\xi\xi} &= \frac{\partial W^{\mathrm{S}}}{\partial \kappa_{\xi\xi}}, \quad m_{\xi\eta} = m_{\eta\xi} = \frac{1}{2}\frac{\partial W^{\mathrm{S}}}{\partial \kappa_{\xi\eta}}, \quad m_{\eta\eta} = \frac{\partial W^{\mathrm{S}}}{\partial \kappa_{\eta\eta}}. \end{aligned} \tag{4.53}$$

For the strain energy function expressed by (4.52),

$$\begin{aligned} \tau_{\xi\xi} &= \frac{Eh}{1-\nu^2}(\epsilon_{\xi\xi} + \nu\epsilon_{\eta\eta}), \quad \tau_{\xi\eta} = \tau_{\eta\xi} = \frac{Eh}{1+\nu}\epsilon_{\xi\eta}, \quad \tau_{\eta\eta} = \frac{Eh}{1-\nu^2}(\epsilon_{\eta\eta} + \nu\epsilon_{\xi\xi}), \\ m_{\xi\xi} &= \frac{1}{12}\frac{Eh^3}{1-\nu^2}(\kappa_{\xi\xi} + \nu\kappa_{\eta\eta}), \quad m_{\xi\eta} = m_{\eta\xi} = \frac{1}{12}\frac{Eh^3}{1+\nu}\kappa_{\xi\eta}, \\ m_{\eta\eta} &= \frac{1}{12}\frac{Eh^3}{1-\nu^2}(\kappa_{\eta\eta} + \nu\kappa_{\xi\xi}). \end{aligned} \tag{4.54}$$

It should be emphasized that the preceding formulae apply only for small interfacial deformations. The recent work of Steigmann and Ogden [173, 174] establishes a framework for computing bending moments for finite deformations. In the nonlinear formulation, the tension tensor τ is decomposed into a symmetric part and a skew-symmetric part defined in Eq. (4.5). Constitutive equations for the symmetric part and for the tensor of bending moments are then developed in terms of a strain energy function of strain and bending measures.

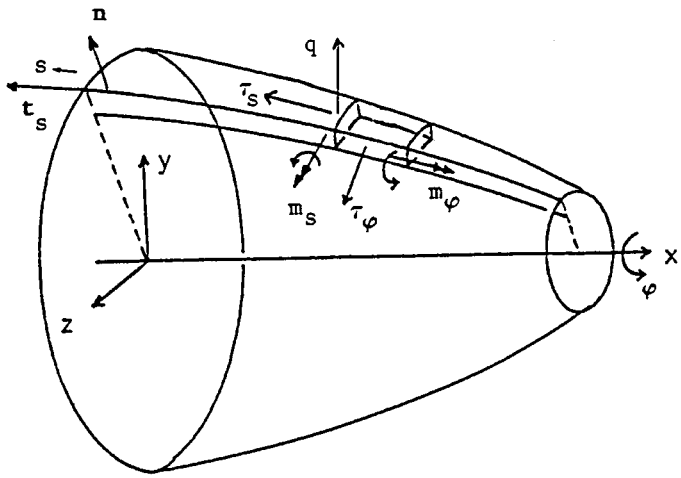

FIG. 5. Elastic tensions and bending moments developing around the edges of a patch on an axisymmetric membrane.

4.9. *Axisymmetric Membranes*

Nest, we turn our attention to axisymmetric membranes generated by rotating a line around the x axis, as depicted in Fig. 5. Kinematics and dynamics are described in polar cylindrical coordinates with axial position x, distance from the x axis, and meridional angle measured around the x axis with origin in the xy plane forming the triplet (x, σ, φ). The flow inside and outside the capsule and the membrane tensions and bending moments developing due to the deformation are assumed to be axisymmetric.

Following the formalism of thin-shell theory, we consider the mid-surface of the membrane and introduce: (a) the azimuthal and meridional tensions τ_s and τ_φ, which are the principal tensions of the in-plane stress resultants, (b) the transverse shear tension q, and (c) the azimuthal and meridional bending moments m_s and m_φ, as illustrated in Fig. 5.

As a preliminary, we introduce the arc length along the trace of the membrane in a meridional plane denoted by s and the unit vector that is tangential to the membrane and lies in a meridional plane corresponding to a certain value of the meridional angle φ, denoted by $\mathbf{t}_s$. The unit vector normal to the interface, $\mathbf{n}$, is directed into the ambient suspending fluid, as illustrated in Fig. 5. The principal curvatures of the membrane in a meridional plane and its conjugate plane are denoted by κ_s and κ_φ.

Using fundamental relations of differential geometry, we find that if the radial position of the membrane is described by the equation

$$\sigma = f(s) = g(x), \tag{4.55}$$

then the principal curvatures are given by

$$\kappa_s = -\frac{f''}{\sqrt{1-f'^2}} = -\frac{g''}{(1+g'^2)^{3/2}} \tag{4.56}$$

and

$$\kappa_\varphi = \frac{1}{\sigma}\frac{\partial x}{\partial s} = \frac{1}{\sigma}\sqrt{1-f'^2} = \frac{1}{\sigma}\frac{1}{\sqrt{1+g'^2}} \tag{4.57}$$

(e.g., Pozrikidis [133, p. 162]). These expressions are consistent with Godazzi's formula

$$\kappa_s = \frac{\partial}{\partial \sigma}(\sigma \kappa_\varphi), \tag{4.58}$$

which allows us to compute one of the principal curvatures in terms of the other.

4.9.1. Force and torque balances. To compute the jump in the hydrodynamic traction across the membrane, we consider a small section of the membrane that is confined between: (a) two meridional planes passing through the x axis, and (b) two parallel planes that are perpendicular to the x axis and enclose a small section of the interface in a meridional plane with arc length Δs. Performing a force balance over this section, we find

$$\Delta \mathbf{f} = \left(\sigma^{(\mathrm{s})} - \sigma^{(\mathrm{c})}\right) \cdot \mathbf{n} = \Delta f^{\mathrm{n}} \mathbf{n} + \Delta f^{\mathrm{s}} \mathbf{t}_s, \tag{4.59}$$

where the normal jump is given by

$$\Delta f^{\mathrm{n}} = \kappa_s \tau_s + \kappa_\varphi \tau_\varphi - \frac{1}{\sigma}\frac{\partial}{\partial s}(\sigma q), \tag{4.60}$$

and the tangential jump is given by

$$\Delta f^{\mathrm{s}} = -\frac{\partial \tau_s}{\partial s} - \frac{1}{\sigma}\frac{\partial f}{\partial s}(\tau_s - \tau_\varphi) - \kappa_s q. \tag{4.61}$$

The function $f(s)$, describing the shape of the membrane, was defined in Eq. (4.55). An analogous torque balance shows that the transverse shear tension is related to the bending moments by

$$q = \frac{1}{\sigma}\frac{\partial}{\partial s}(\sigma m_s) - m_\varphi \frac{1}{\sigma}\frac{\partial f}{\partial s} = \frac{1}{\sigma}\frac{\partial f}{\partial s}\left(\frac{\partial}{\partial \sigma}(\sigma m_s) - m_\varphi\right) \tag{4.62}$$

(e.g., Møllmann) [108, p. 33]. Substituting the right-hand side of (4.62) in place of the shear tension in (4.60) and (4.61), we obtain relations in terms of the in-plane stress resultants and bending moments alone.

It is reassuring to confirm that expressions (4.60)–(4.62) are consistent with the more general expressions for three-dimensional membranes discussed earlier in this section. For this purpose, we identify the surface curvilinear coordinate ξ with the arc length measured along the trace of the membrane in a meridional plane denoted by s, and the curvilinear coordinate η with the meridional angle φ, whereupon the arc length metric coefficients are given by $h_\xi = 1$ and $h_\eta = \sigma$. Since all tensions and moments have been assumed axisymmetric, the principal axes coincide with the chosen curvilinear axes, and Eqs. (4.15)–(4.20) reproduce Eqs. (4.60)–(4.62).

To evaluate the right-hand side of Eqs. (4.60)–(4.62), we require constitutive relations for the elastic stress resultants and bending moments.

4.9.2. Constitutive equations for the elastic tensions. To derive relations for the elastic tensions, we introduce the principal extension ratios

$$\lambda_s = \frac{\partial s}{\partial s^{\mathrm{R}}}, \quad \lambda_\varphi = \frac{\sigma}{\sigma^{\mathrm{R}}}, \tag{4.63}$$

where the superscript R denotes a reference state. If the area of the membrane is locally and thus globally conserved,

$$\lambda_s \lambda_\varphi = 1. \tag{4.64}$$

To this end, we have two main choices reflecting the assumed nature of the membrane.

First, we may regard the membrane as a distinct two-dimensional hyperelastic medium, and express the principal stress resultants in terms of the surface strain energy function W^{S} using equations (4.35), where $\tau_1^{\mathrm{P}} = \tau_s$, $\tau_2^{\mathrm{P}} = \tau_\varphi$, $\lambda_1 = \lambda_s$, and $\lambda_2 = \lambda_\varphi$. Alternatively, we may regard the membrane as a thin sheet of a three-dimensional incompressible material and work with the strain invariants shown in (4.46); the principal elastic tensions derive from the volume strain energy function W^{V} using relations (4.47).

4.9.3. Constitutive equations for bending moments. To compute the bending moments developing in a hyperelastic membrane, we introduce the bending measures of strain

$$K_s = \lambda_s \kappa_s - \kappa_s^{\mathrm{R}}, \quad K_\varphi = \lambda_\varphi \kappa_\varphi - \kappa_\varphi^{\mathrm{R}}, \tag{4.65}$$

where the superscript R denotes a reference configuration corresponding to the unstressed shape where the bending moments vanish [151–154]. Zarda *et al.* [202] expressed the bending moments in terms of the surface bending energy function W_{B} in a form that is analogous to that shown in Eqs. (4.35), as

$$m_s = \frac{1}{\lambda_\varphi} \frac{\partial W_{\mathrm{B}}}{\partial K_s}, \quad m_\varphi = \frac{1}{\lambda_s} \frac{\partial W_{\mathrm{B}}}{\partial K_\varphi}. \tag{4.66}$$

Love's first approximation given by the last expression on the right-hand side of (4.52) yields the bending energy function

$$W_{\mathrm{B}} = \frac{E_{\mathrm{B}}}{2} \left(K_s^2 + 2\nu K_s K_\varphi + K_s^2 \right), \tag{4.67}$$

where E_{B} and ν are physical constants expressing membrane material properties.

5. INCOMPRESSIBLE INTERFACES

Biological, membranes consisting of lipid bilayers have a large modulus of dilatation; that is, they behave like two-dimensional nearly-incompressible fluids. To account for the membrane incompressibility, a position-dependent isotropic tension playing the role of surface pressure may be added to the in-plane stress resultants. The introduction of an additional surface function furnishes an additional degree of freedom that allows the satisfaction of the incompressibility constraint at every point over the membrane.

In global Cartesian coordinates, the incompressibility constraint is expressed by the equation

$$\theta = \frac{1}{h_S} \frac{D h_S}{D t} = (\mathbf{P} \cdot \nabla) \cdot \mathbf{u} = 0, \tag{5.1}$$

where θ is the rate of surface dilatation, D/Dt is the material derivative, h_s is the surface metric associated with the convected surface curvilinear coordinates, and $\mathbf{u}$ is the fluid velocity [162].

In surface curvilinear coordinates (ξ, η), the incompressibility constraint (6.1) takes the form

$$\theta = \frac{1}{h_S}\frac{Dh_S}{Dt} = \frac{1}{h_S}\mathbf{n}\cdot\left(\frac{\partial \mathbf{u}}{\partial \xi}\times\frac{\partial \mathbf{x}}{\partial \eta} + \frac{\partial \mathbf{x}}{\partial \xi}\times\frac{\partial \mathbf{u}}{\partial \eta}\right)$$
$$= (\mathbf{P}\cdot\nabla)\cdot(\mathbf{P}\cdot\mathbf{u}) + 2\,\kappa_m\mathbf{u}\cdot\mathbf{n} = 0 = u^{\xi}|_{\xi} + u^{\eta}|_{\eta} + 2\,\kappa_m\mathbf{u}\cdot\mathbf{n} = 0, \qquad (5.2)$$

where κ_m is the interface mean curvature [133, p. 21; 193, Eq. 3.2b; 208]. A vertical bar signifies the covariant derivative taken with respect to the subscribed variable, defined in terms of the Christoffel symbols (e.g., [5]). Condition (5.2) also follows from the convection–diffusion equation for a uniformly distributed insoluble surfactant, equation (3.19), by requiring that the surfactant concentration at the position interfacial point particles moving with the fluid velocity remains constant in time. The numerical implementation of (5.2) for capsules deforming under the influence of a simple shear flow was discussed by Zhou and Pozrikidis [208].

Considering axisymmetric flow, we express the azimuthal and meridional tensions in terms of a mean and a deviatoric component; the latter derives from a strain energy function. Pozrikidis [126] simulated the transient deformation of axisymmetric capsules enclosed by incompressible elastic membranes evolving under the influence of an elongational flow. The distribution of the isotropic membrane tension was computed using the incompressibility constraint (5.2), and the deviatory elastic tension was computed using a constitutive equation. Requiring $D(\lambda_s\lambda_\varphi)/Dt = 0$, where D/Dt is the material derivative, we obtain a scalar constraint on the distribution of the membrane velocity $\mathbf{u}$,

$$\mathbf{t}_s\cdot\frac{\partial \mathbf{u}}{\partial s} + \frac{1}{\sigma}\,\mathbf{u}\cdot\mathbf{e}_\sigma = 0, \qquad (5.3)$$

where $\mathbf{t}_s$ is the unit vector tangential to the membrane in a meridional plane, and $\mathbf{e}_\sigma$ is the unit vector normal to the x axis. It can be shown by straightforward rearrangement that condition (5.3) is consistent with the more general expressions (5.1) and (5.2).

In the case of two-dimensional flow, the incompressibility constraint simplifies to

$$\mathbf{t}\cdot\frac{\partial \mathbf{u}}{\partial l} = \frac{\partial(\mathbf{u}\cdot\mathbf{t})}{\partial l} + \kappa\mathbf{u}\cdot\mathbf{n} = 0, \qquad (5.4)$$

where $\mathbf{t}$ is the unit vector tangential to the membrane, l is the arc length measured in the direction of $\mathbf{t}$, and κ is the curvature of the membrane in the xy plane. The numerical implementation of (5.4) is discussed by Zhou and Pozrikidis [208].

6. VISCOUS INTERFACES

Impurities, surfactants, adsorbed macromolecules, and molecular layers generated by chemical reactions are responsible for interfaces that behave like two-dimensional Newtonian or viscoelastic Boussinesq fluids (e.g., [161, 193, 10, 170, 36, 110]). Scriven [161] proposed a constitutive equation for in-plane Newtonian interfacial tensions in surface curvilinear coordinates. Secomb and Skalak [162] observed that the coupling of the interfacial dynamics to the hydrodynamics on either side of the interface is facilitated by working in global Cartesian coordinates and expressed the Newtonian surface tension tensor

in the form

$$\tau = \gamma\, \mathbf{P} + (\kappa - \epsilon)\, \theta\, \mathbf{P} + 2\, \epsilon\, \mathbf{E}^{\mathrm{S}}, \tag{6.1}$$

where θ is the rate of dilatation given in Eqs. (5.1) and (5.2), $\mathbf{P} = \mathbf{I} - \mathbf{nn}$ is the tangential projection operator, ϵ and κ are two physical constants expressing the interface shear and dilatational viscosity, and $\mathbf{E}^{\mathrm{S}}$ is the Cartesian surface rate of deformation tensor given by

$$E^{\mathrm{S}}_{ij} = \frac{1}{2} P_{ik} P_{jl} \left(\frac{\partial u_k}{\partial x_l} + \frac{\partial u_l}{\partial x_k} \right). \tag{6.2}$$

The two projections on the right-hand side of (6.2) remove derivatives of the velocity in the direction normal to the interface, as well derivatives of the normal component of the velocity in directions that are tangential to the interface. Thus, the right-hand side of (6.2) may be computed from knowledge of the velocity distribution over the interface. The rate of surface dilation θ is given by the trace of $\mathbf{E}^{\mathrm{S}}$.

Performing a force balance over a small interfacial patch, and taking the limit as the size of the patch becomes infinitesimal, we find that the jump in the hydrodynamic traction is given by

$$\Delta \tilde{\mathbf{f}} = -(\mathbf{P} \cdot \nabla) \cdot \tau. \tag{6.3}$$

Substituting this expression into the boundary-integral equation, we obtain an integral equation of a nonstandard kind for the interfacial velocity [130].

7. COMPLEX INTERFACES AND ALTERNATIVE FORMULATIONS

We have discussed the mathematical modeling of membrane tensions and bending moments in the context of continuum mechanics, working under the auspices of the theory of thin shells. The macromolecular nature of certain interfaces suggests that an alternative formulation that models a membrane as a network of generally viscoelastic links defined by computational nodes might be more appropriate. For example, Hansen *et al.* [54–56] developed a network model based on random Delaunay triangulation representing the erythrocyte membrane cytoskeleton and obtained estimates for the macroscopic elastic shear modulus and modulus of areal expansion.

An alternative method of computing the jump in the hydrodynamic traction across an interface hinges on the concept of configurational energy playing the role of an effective Hamiltonian (e.g., [2, 21, 112]). For example, the instantaneous configurational energy of a membrane consisting of a symmetric lipid bilayer may be expressed in terms of surface integrals in the form

$$E = \int_{\text{Membrane}} \tau\, dS + 2\, \kappa_{\mathrm{B}} \int_{\text{Membrane}} \kappa_m^2\, dS, \tag{7.1}$$

where κ_{B} is a physical constant expressing the bending stiffness, κ_m is the membrane mean curvature, and τ is a position dependent in-plane tension developing to ensure membrane incompressibility [163]. Let the instantaneous shape of the membrane be described by the equation $G(\mathbf{x}) = 0$, where G is a suitable function, and express the interface energy in the

form $E = E(G(\mathbf{x}))$ evaluated at $G(\mathbf{x}) = 0$, where $E(\cdot)$ is a nonlinear integro-differential functional defined over all possible membrane configurations. The jump in the hydrodynamic traction across the membrane may be found using the principle of virtual displacements (e.g., [112]).

Kraus *et al.* [69] discretized the membrane of a vesicle into a collection of flat triangles defined by computational nodes, represented the flow by a superposition of elementary flows induced by point forces located at the triangle vertices, and computed the strength of the point force located at the jth node, denoted by $\mathbf{x}^{(j)}$, by the equation

$$F_i^{(j)} = -\frac{\partial E}{\partial x_i^{(j)}}, \tag{7.2}$$

which is the simplest implementation of the principle of virtual displacements. Although computationally convenient, discrete models are sensitive to the method of surface discretization–flat versus curved triangulation.

Boey *et al.* [15] and Discher *et al.* [33] developed a coarse-grained molecular model that permits the direct coupling of classical hydrodynamics to the dynamics of the molecular layers and networks comprising the membrane, in a manner that circumvents the explicit use of a macroscopic constitutive equation (see also Seifert [163]).

8. INTERFACIAL DYNAMICS

An integrated numerical procedure for simulating the evolution of interfaces using a boundary-integral method involves three main tasks: (a) parametric representation of the interfaces; (b) evaluation of an integral representation or solution of an integral equation for the interfacial velocity or for the density of a hydrodynamic potential; and (c) time integration of the equations governing the motion of interfacial marker points and possibly the evolution of dynamically relevant surface functions. In the case of temperature- or surfactant-concentration-dependent surface tension, dynamically relevant surface functions include the temperature and the concentration of a surfactant. In the case of an interface consisting of an elastic membrane, dynamically relevant surface functions include the coordinates and the curvature of the interface at the position of marker points in a reference configuration. The overall numerical method is described as the method of interfacial dynamics for Stokes flow.

The implementation of the aforementioned tasks is considerably faciliated by the use of piecewise numerical interpolation underlying the formalism of boundary-element methods. In the case of two-dimensional or axisymmetric flow, an interface is represented by a collection of planar elements in the form of straight segments, circular arcs, parabolic, cubic, cubic-spline, or higher order elements, all defined by consecutive interfacial nodes. The cubic-spline elements are described in parametric form by means of cubic-spline interpolation for the node coordinates, where the interpolation is done with respect to the polygonal or curved arc length [136]. The geometrical properties of the interface including the normal vector and the curvature follow readily from the local representation.

In the case of three-dimensional flow, an interface is typically represented by an unstructured grid of three-dimensional elements defined by groups of interfacial nodes. Compared to a structured grid defined in global curvilinear coordinates, the unstructured grid has two advantages: the local curvilinear coordinates over each element are nonsingular, whereas the structured grid may have singular points; and the element shape and size may be readily

controlled to enhance the spatial resolution at selected regions. The unstructured discretization is amenable to the meritorious finite-volume and finite-element formulations for solving integral and differential equations over evolving domains. Flat and curved riangular elements are particularly attractive because of their ease of implementation. A closed grid of triangles may be readily generated by successively subdividing a regular octahedron or icosahedron into four descendant elements, and subsequently deforming the elements to obtain a desired shape [139].

8.1. *Computation of the Normal Vector and Mean Curvature*

The unit normal vector and mean curvature of a two-dimensional or axisymmetric interface follow readily from the parametric representation using standard formulae of differential geometry (e.g., [133]).

A simple method for computing the unit normal vector and mean curvature of a three-dimensional interface is by evaluating a contour integral. Consider an interfacial patch D enclosed by the contour C and containing the point $\mathbf{x}_0$, and introduce the unit vector $\mathbf{b}$ that is tangential to the patch and lies in a plane that is normal to C at a point, as shown in Fig. 2. If $\mathbf{t}$ is the unit vector tangential to C, and $\mathbf{n}$ is the unit vector normal to the interface, then $\mathbf{b} = \mathbf{t} \times \mathbf{n}$. In the limit as the contour C shrinks to the point $\mathbf{x}_0$, the reduced vectorial line integral

$$\mathbf{a}(\mathbf{x}_0) \equiv \frac{1}{S_D} \int_C \mathbf{b}(\mathbf{x})\, dl(\mathbf{x}), \tag{8.1}$$

tends to the vector $2\,\kappa_m(\mathbf{x}_0)\,\mathbf{n}(\mathbf{x}_0)$, where κ_m is the mean curvature of the interface at the point $\mathbf{x}_0$, and S_D is the surface area of D. The unit normal vector $\mathbf{n}(\mathbf{x}_0)$ follows by normalizing the vector $\mathbf{a}(\mathbf{x}_0)$, possibly switching its direction to ensure that has a desired orientation; the mean curvature follows from the inner product $\mathbf{a}(\mathbf{x}_0) \cdot \mathbf{n}(\mathbf{x}_0) \equiv 2\,\kappa_m(\mathbf{x}_0)$ (e.g., [127, 128]). In practice, the contour C is identified either with jointed sections of surface curvilinear coordinates defining a surface element, or with groups of selected edges of boundary elements in the vicinity of a point.

When an interface has been discretized into flat triangles, the computation of the normal vector and mean curvature requires interpolating beyond the domain of the individual elements. Rallison [148] described the shape of an interface in the vicinity of a node by the equation $f(\mathbf{x}) = 0$, expanded the function $f(\mathbf{x})$ in a Taylor series, truncated the series at the quadratic term, and computed the unknown coefficients using a numerical method. Zinchenko *et al.* [210, 211] approximated the interface in the vicinity of a node with a paraboloid defined in local Cartesian coordinates with one axis normal to the interface at the node. The coefficients of the local paraboloid were computed by minimization, and the normal vector was improved by iteration; upon convergence, the mean curvature followed from standard expressions. Zinchenko found that the contour integration method discussed in the preceding paragraph suffers from serious flaws even for simple ellipsoidal shapes. An improved version of the local paraboloidal approximation that produces the normal vector and the mean curvature simultaneously by global minimization was developed recently by Zinchenko and Davis [209]. Tests showed that the global method produces more accurate normal vectors, but not necessarily more accurate mean curvatures.

When an interface has been discretized into quadratic triangular element defined by six nodes, the normal vector, directional normal curvatures, and mean curvature follow readily

from the local parametric representation of the individual elements (Pozrikidis [127, 136, 139]; Kennedy *et al.* [65]). The mean curvature, in particular, may be computed as the ratio of the first to the second fundamental form of the surface defined in Eqs. (4.8) and (4.10). The following recipe gives the best results: (a) compute the normal vector at the nodes of each triangle using the local triangle representation; (b) average the components of the normal vector over all triangles sharing a node; (c) normalize the averaged normal vector; (d) compute the surface gradient of the averaged normal vector over each triangle using the local triangle representation; (e) compute the mean curvature at a specified point over a triangle as the ratio of the first to the second fundamental form of the surface. When a sphere has been discretized into eight quadratic triangles, the method just described produces the mean curvature without any numerical error!

8.2. *Computation of the Singular Single-Layer Potential*

Two distinct but somewhat related issues arise in the computation of the single-layer potential: (a) the accurate evaluation of the jump in interfacial traction $\Delta\mathbf{f}$, and (b) the accurate evaluation of the singular integral. The two issues are related in the sense that specialized methods for computing the single-layer potential may be devised for particular expressions for $\Delta\mathbf{f}$.

In the case of two-dimensional or axisymmetric flow, the kernel of the single-layer potential exhibits a logarithmic singularity which may be integrated by several methods, including the use of a Gaussian quadrature for a log-singular (e.g., [136]). In the case of three-dimensional flow, the kernel of the single-layer potential exhibits a weak singularity that behaves as $1/r$. Quadratures for integrating the single-layer potential over planar triangles and rectangles have been developed by Pina *et al.* [119]. A recent monograph edited by Sladek and Sladek [170] reviews methods for computing weakly and selected strongly singular integrals in boundary-element implementations. In this section, we discuss selected strategies pertinent to the integral equations of Stokes flow.

8.2.1. Isolating the jump in traction. Let us consider the single-layer potential over an interfacial patch D that is enclosed by the closed contour C, and introduce the single-layer potential

$$I_j^{\mathrm{S}}(\mathbf{x}_0) \equiv \int_D G_{ij}(\mathbf{x}, \mathbf{x}_0)\, \Delta f_i(\mathbf{x})\, dS(\mathbf{x}). \tag{8.2}$$

Implementing a trapezoidal-like approximation to decouple the product of the two functions in the integrand, we write

$$I_j^{\mathrm{S}}(\mathbf{x}_0) \simeq \frac{1}{S_D} \int_D \Delta f_i(\mathbf{x})\, dS(\mathbf{x}) \times \int_D G_{ij}(\mathbf{x}, \mathbf{x}_0)\, dS(\mathbf{x}), \tag{8.3}$$

where S_D is the surface area of D. Assuming that the interface develops in-plane and transverse shear tensions, as discussed in Section 4, we perform a force balance over the patch to find that the first integral on the right-hand side of (8.3) is given by

$$\int_D \Delta\mathbf{f}(\mathbf{x})\, dS(\mathbf{x}) = -\int_D \mathbf{b}(\mathbf{x}) \cdot [\tau(\mathbf{x}) + \mathbf{q}(\mathbf{x})\, \mathbf{n}(\mathbf{x})]\, dl(\mathbf{x}). \tag{8.4}$$

For example, if the interface exhibits uniform isotropic tension γ, $\tau = \gamma\, \mathbf{P}$ and $\mathbf{q} = \mathbf{0}$, where $\mathbf{P} = \mathbf{I} - \mathbf{nn}$ is the tangential projection operator; in this case, $\mathbf{b} \cdot \tau = \gamma \mathbf{b}$.

The computation of the right-hand side of (8.4) requires the evaluation of the in-plane surface tension tensor τ and transverse shear tension vector $\mathbf{q}$ along the contour C. In contrast, the computation of $\Delta\mathbf{f}$ in the integrand on the left-hand side of (8.4) requires the evaluation of the surface divergence or gradient of τ and $\mathbf{q}$ over D, which can be a serious source of numerical error. The approximation (8.3) was implemented by Pozrikidis [129] for interfaces with isotropic tension, and by Pozrikidis [131], Ramanujan and Pozrikidis [150], and Pozrikidis [144] for interfaces developing in-plane and transverse shear tensions.

8.2.2. Integration of the normal component of $\Delta\mathbf{f}$. The jump in traction $\Delta\mathbf{f}$ may be decomposed into a normal and a tangential component, as

$$\Delta\mathbf{f} = \chi\,\mathbf{n} + \mathbf{P}\cdot\Delta\mathbf{f}, \tag{8.5}$$

where $\chi = \mathbf{n}\cdot\Delta\mathbf{f}$. Each component may then be integrated independently using different methods. For example, if an interface exhibits uniform tension γ, $\chi = \gamma 2\kappa_m$ where κ_m is the mean curvature, and the tangential component vanishes.

If an interface is closed, the single-layer integral associated with the normal component of $\Delta\mathbf{f}$ may be removed by use of an integral identity: conservation of mass for the flow due to a point force allows us to write

$$\int_D G_{ij}(\mathbf{x},\mathbf{x}_0)\,\chi(\mathbf{x})\,n_i(\mathbf{x})\,dS(\mathbf{x}) = \int_D G_{ij}(\mathbf{x},\mathbf{x}_0)\,[\chi(\mathbf{x})-\chi(\mathbf{x}_0)]\,n_i(\mathbf{x})\,dS(\mathbf{x}). \tag{8.6}$$

The integrand on the right-hand of (8.6) is nonsingular but not entirely regular. A Taylor series expansion shows that as the integration point $\mathbf{x}$ approaches the evaluation point $\mathbf{x}_0$, the integrand tends to a finite value that depends on the orientation of the vector $\mathbf{x}-\mathbf{x}_0$. In practice, however, this integral may be computed with adequate accuracy using an integration quadrature for regular integrands (e.g., Pozrikidis [136, pp. 370–383]). An analogous method for removing the singularity of the tangential component $\mathbf{P}\cdot\Delta\mathbf{f}$ by use of an integral identity is not available.

8.2.3. Direct numerical computation of the single-layer integral. In a typical boundary-element implementation, a three-dimensional interface is discretized into a collection of boundary elements, and the single-layer potential is computed over the individual elements. When the evaluation point $\mathbf{x}_0$ lies in the interior, along the edges, or at the vertices of a boundary element, then as the integration point $\mathbf{x}$ approaches $\mathbf{x}_0$, the integrand exhibits a weak $1/|\mathbf{x}-\mathbf{x}_0|$ singularity, and the element is classified as "singular."

To compute the single-layer potential over a singular element E, we write

$$I_j^{\mathrm{S}}(\mathbf{x}_0) = \int_D G_{ij}(\mathbf{x},\mathbf{x}_0)[\Delta f_i(\mathbf{x})-\Delta f_i(\mathbf{x}_0)]\,dS(\mathbf{x}) + \Delta f_i(\mathbf{x}_0)\int_D G_{ij}(\mathbf{x},\mathbf{x}_0)\,dS(\mathbf{x}). \tag{8.7}$$

As the integration point $\mathbf{x}$ approaches the evaluation point $\mathbf{x}_0$, the integrand of the first integral on the right-hand side of (8.7) tends to a finite value that depends on the orientation of the vector $\mathbf{x}-\mathbf{x}_0$, and the integral may be computed with adequate accuracy using a standard quadrature.

When the elements are flat triangles, and the point $\mathbf{x}_0$ is a vertex, the second integral on the right-hand side of (8.7) may be computed by analytical methods [27, 148]. A practical alternative is to use the polar integration rule, which amounts to integrating in local polar

coordinates using a double Gauss–Legendre quadrature (e.g., Pozrikidis [136, pp. 377–388]). A third option is to use a Gauss quadrature for two-dimensional integrals with a $1/r$ singularity developed by Pina *et al.* [119].

To compute the single-layer potential over an element that is defined by more than three nodes, such as a curved triangle defined by six nodes, we break up the element into a collection of flat triangles according to the location of the singular point $\mathbf{x}_0$, and then either perform the integration analytically, use the polar integration rule for singular flat triangles described earlier in this section, or employ an integration quadrature. For example, if the evaluation point lies at the vertex of aquadratic triangle defined by six nodes, the quadratic triangle is broken up into one singular flat triangle and three nonsingular flat triangles.

8.3. *Computation of the Principal-Value Integral of the Double-Layer Potential*

In the case of two-dimensional or axisymmetric flow, the integrand of the principal-value integral of the double-layer potential is nonsingular and may be computed using a standard numerical method. In the case of three-dimensional flow, the $1/|\mathbf{x}-\mathbf{x}_0|$ singularity of the principal value integral over a *closed* surface may be removed using a vector identity, writing

$$\begin{aligned} I_j^D(\mathbf{x}_0) &\equiv \int_D^{\mathrm{PV}} q_i(\mathbf{x})\, T_{ijk}(\mathbf{x},\mathbf{x}_0)\, n_k(\mathbf{x})\, dS(\mathbf{x}) \\ &= \int_D [q_i(\mathbf{x}) - q_i(\mathbf{x}_0)]\, T_{ijk}(\mathbf{x},\mathbf{x}_0)\, n_k(\mathbf{x})\, dS(\mathbf{x}) - 4\pi\, q_j(\mathbf{x}_0), \end{aligned} \tag{8.8}$$

where $\mathbf{q}$ is the density of the double-layer potential (e.g., Pozrikidis [127]). As the integration point $\mathbf{x}$ approaches the evaluation point $\mathbf{x}_0$, the integrand on the right-hand side of (8.8) tends to a finite value that depends on the orientation of the vector $\mathbf{x}-\mathbf{x}_0$; the integral may be computed with adequate accuracy using a standard quadrature. A similar regularization may be performed when the point $\mathbf{x}_0$ lies close to, but not precisely on the domain of integration D (Loewenberg & Hinch [91, 92]; Zinchenko *et al.* [209, 210]; Zinchenko & Davis [211]).

When the domain of integration is not closed, the computation of the double-layer potential becomes more challenging. Use of the polar integration rule to integrate over a flat triangle, as discussed earlier for the single-layer potential, removes the $1/|\mathbf{x}-\mathbf{x}_0|$ singularity and allows the application of a standard quadrature. Because, however, the kernel $T_{ijk}n_k$ of the free-space Green's function vanishes over a flat element hosting the singular point, neglecting the surface curvature introduces a significant numerical error on the order of $\kappa_m\,\delta$, where κ_m is the mean curvature and δ is the element size. The implementation of the polar integration rule over curved elements is cumbersome and has not been attempted. One way to bypass these difficulties is to introduce the closure of an open interface, and then compute the nonsingular double-layer integral over the extended boundary using a quadrature [199]. Other methods are discussed in the articles collected by Sladek and Sladek [170].

8.4. *Computation of the Principal Value of the Point-Source Integral*

We consider now the computation of the principal value of the first integral on the right-hand sides of (3.12), named the point-source integral. This integral also arises in the study of the self-induced motion of vortex sheets with particular reference to the Biot–Savart integral (e.g., Pozrikidis [133]).

Considering, for simplicity, an interface with constant surface tension γ, we define the point source potential

$$I_j^{\mathrm{PS}}(\mathbf{x}_0) = \int_D^{\mathrm{PV}} p_j(\mathbf{x}, \mathbf{x}_0)\, dS(\mathbf{x}). \tag{8.9}$$

As the integration point $\mathbf{x}$ approaches the evaluation point $\mathbf{x}_0$, the integrand on the right-hand side of (8.9) exhibits a strong singularity, behaving like $1/|\mathbf{x} - \mathbf{x}_0|^2$. Our objective is to reduce the order of the singularity by use of integral identities.

For the purpose of illustration, we confine our attention to the free-space pressure Green's function given by $p_j(\mathbf{x}, \mathbf{x}_0) = 2\,\hat{x}_j/|\hat{\mathbf{x}}|^3$, where $\hat{\mathbf{x}} \equiv \mathbf{x} - \mathbf{x}_0$. An arbitrary pressure Green's functions may be decomposed into a singular part associated with the free-space Green's function and a regular complementary part, and the latter may be integrated using standard numerical methods.

To simplify the notation, we write $p_j = -8\pi \nabla G^{\mathrm{L}}$, where G^{L} is the free-space Green's function of Laplace's equation given by $G^{\mathrm{L}}(\mathbf{x}, \mathbf{x}_0) = 1/(4\pi|\hat{\mathbf{x}}|)$, Substituting this form into (8.9), we find $\mathbf{I}^{\mathrm{PS}}(\mathbf{x}_0) = -8\pi\, \mathbf{I}^{\mathrm{GL}}(\mathbf{x}_0)$, where

$$\mathbf{I}^{\mathrm{GL}}(\mathbf{x}_0) \equiv \int_D^{\mathrm{PV}} \nabla G^{\mathrm{L}}(\mathbf{x}, \mathbf{x}_0)\, dS(\mathbf{x}) = -\left[\nabla_0 \int_D G^{\mathrm{L}}(\mathbf{x}, \mathbf{x}_0)\, dS(\mathbf{x})\right]^{\mathrm{PV}} \tag{8.10}$$

is the principal value of the gradient of the Laplace potential. The derivatives of the gradient ∇_0 on the right-hand side of (8.10) are taken with respect to $\mathbf{x}_0$. The compute the gradient of the Laplace potential, we may proceed in two ways.

In the first approach, we decompose the kernel ∇G^{L} into its normal and tangential components, and write

$$\begin{aligned}\mathbf{I}^{\mathrm{GL}}(\mathbf{x}_0) = &\int_D [\mathbf{n}(\mathbf{x}) - \mathbf{n}(\mathbf{x}_0)]\, \mathbf{n}(\mathbf{x}) \cdot \nabla G^{\mathrm{L}}(\mathbf{x}, \mathbf{x}_0)\, dS(\mathbf{x}) + \mathbf{n}(\mathbf{x}_0) \int_D \mathbf{n}(\mathbf{x}) \cdot \nabla G^{\mathrm{L}}(\mathbf{x}, \mathbf{x}_0)\, dS(\mathbf{x}) \\ &+ \int_D^{\mathrm{PV}} \mathbf{P}(\mathbf{x}) \cdot \nabla G^{\mathrm{L}}(\mathbf{x}, \mathbf{x}_0)\, dS(\mathbf{x}),\end{aligned} \tag{8.11}$$

where $\mathbf{P} = \mathbf{I} - \mathbf{nn}$ is the tangential projection operator. As the integration point $\mathbf{x}$ approaches the evaluation point $\mathbf{x}_0$, the kernel of the first integral on the left-hand side of (8.11) tends to a finite value that depends on the direction of $\mathbf{x} - \mathbf{x}_0$. The integral may be computed with adequate accuracy using a standard integration quadrature. Conservation of mass for the flow due to point sink requires that the second integral on the left-hand side is equal to $-1/2$. Pozrikidis [142] shows that the third integral on the right-hand side of (8.12) is equal to

$$\int_D 2\,\kappa_m(\mathbf{x})\, G^{\mathrm{L}}(\mathbf{x}, \mathbf{x}_0)\, \mathbf{n}(\mathbf{x})\, dS(\mathbf{x}), \tag{8.12}$$

where κ_m is the mean curvature of D. Since the kernel of this integral diverges only weakly as $1/|\mathbf{x} - \mathbf{x}_0|$, the integral may be computed with adequate accuracy using a numerical method that is analogous to that described earlier for the single-layer Stokes potential involving, for example, the polar integration rule.

In the second approach developed by Zinchenko and co-workers [209–211], the gradient of the Laplace integral is decomposed into a normal and a tangential component, and each component is treated individually. To compute the principal value of the normal component,

we express it in the form

$$\mathbf{n}(\mathbf{x}_0)[\mathbf{n}(\mathbf{x}_0)\cdot\mathbf{I}^{\mathrm{GL}}(\mathbf{x}_0)] = \mathbf{n}(\mathbf{x}_0)\int_D [\mathbf{n}(\mathbf{x})+\mathbf{n}(\mathbf{x}_0)]\cdot\nabla G^{\mathrm{L}}(\mathbf{x},\mathbf{x}_0)\,dS(\mathbf{x}) - \mathbf{n}(\mathbf{x}_0)\int_D{}^{\mathrm{PV}}\,\mathbf{n}(\mathbf{x})\cdot\nabla G^{\mathrm{L}}(\mathbf{x},\mathbf{x}_0)\,dS(\mathbf{x}). \tag{8.13}$$

As the integration point $\mathbf{x}$ approaches the singular point $\mathbf{x}_0$, the kernel of the first integral on the left-hand side of (8.13) tends to a finite value that depends on the direction of $\mathbf{x}-\mathbf{x}_0$ (Zinchenko *et al.* [210, p. 1503]). In fact, when the integration domain is a sphere, this integrand vanishes identically at every point. A formal proof that involves expanding the position and normal vector in Taylor series with respect to surface curvilinear coordinates was provided by Zinchenko to this author in personal communication. Conservation of mass for the flow due to point sink requires that the second integral on the left-hand side of (8.13) is equal to $-1/2$.

To compute the tangential component of the gradient of the Laplace potential, we may proceed in two ways. In the indirect approach, we evaluate the last integral of the Green's function in (8.10) over the interface, and then compute its tangential gradient by numerical differentiation, as discussed by Baker [6] and Baker *et al.* [7] and implemented by Pozrikidis [142, 143]. In the direct approach, we express the tangential component in the form

$$\begin{aligned}\mathbf{n}(\mathbf{x}_0)\times[\mathbf{I}^{\mathrm{GL}}(\mathbf{x}_0)\times\mathbf{n}(\mathbf{x}_0)] &= \int_D \mathbf{n}(\mathbf{x}_0)\times[\nabla G^{\mathrm{L}}(\mathbf{x},\mathbf{x}_0)\times\mathbf{n}(\mathbf{x}_0)]\,dS(\mathbf{x})\\ &= \int_D \mathbf{n}(\mathbf{x}_0)\times\{\nabla G^{\mathrm{L}}(\mathbf{x},\mathbf{x}_0)\times[\mathbf{n}(\mathbf{x}_0)-\mathbf{n}(\mathbf{x})]\}\,dS(\mathbf{x})\\ &\quad -\mathbf{n}(\mathbf{x}_0)\times\int_D \mathbf{n}(\mathbf{x})\times\nabla G^{\mathrm{L}}(\mathbf{x},\mathbf{x}_0)\,dS(\mathbf{x}).\end{aligned} \tag{8.14}$$

Expressing the outer triple product within the first integral on the right-hand side of (8.14) in terms of two inner products, we find that, as the integration point $\mathbf{x}$ approaches the singular point $\mathbf{x}_0$, the kernel tends to a finite value that depends on the direction of $\mathbf{x}-\mathbf{x}_0$ [211]. Using the divergence theorem to convert the second integral on the right-hand side of (8.14) to a volume integral over the region enclosed by D, we find that this integral vanishes.

Combining Eqs. (8.13) and (8.14), we derive an expression for the principal value of the gradient of the Laplace potential in terms of a nonsingular integral,

$$\mathbf{I}^{\mathrm{GL}}(\mathbf{x}_0) = \mathbf{n}(\mathbf{x}_0)\int_D [\mathbf{n}(\mathbf{x})+\mathbf{n}(\mathbf{x}_0)]\cdot\nabla G^{\mathrm{L}}(\mathbf{x},\mathbf{x}_0)\,dS(\mathbf{x}) + \int_D \mathbf{n}(\mathbf{x}_0)\times\{\nabla G^{\mathrm{L}}(\mathbf{x},\mathbf{x}_0)\times[\mathbf{n}(\mathbf{x}_0)-\mathbf{n}(\mathbf{x})]\}\,dS(\mathbf{x}) + \frac{1}{2}\,\mathbf{n}(\mathbf{x}_0) \tag{8.15}$$

or

$$\mathbf{I}^{\mathrm{GL}}(\mathbf{x}_0) = \int_D \{[\mathbf{n}(\mathbf{x}_0)\mathbf{n}(\mathbf{x})+\mathbf{n}(\mathbf{x})\mathbf{n}(\mathbf{x}_0)]\cdot\nabla G^{\mathrm{L}}(\mathbf{x},\mathbf{x}_0) + [1-\mathbf{n}(\mathbf{x}_0)\cdot\mathbf{n}(\mathbf{x})]\,\nabla G^{\mathrm{L}}(\mathbf{x},\mathbf{x}_0)\}\,dS(\mathbf{x}) + \frac{1}{2}\,\mathbf{n}(\mathbf{x}_0). \tag{8.16}$$

The right-hand side of (8.16) involves a nonsingular but multivalued integrand.

Considering now the single-layer potential (3.10) for constant surface tension γ, we use (8.16) to express it in the form

$$I_j^s(\mathbf{x}_0) = 4\pi\gamma \int_D \Big\{ n_j(\mathbf{x}_0)\,[\mathbf{n}(\mathbf{x})\cdot\nabla G^{\mathrm{L}}(\mathbf{x},\mathbf{x}_0)] + n_j(\mathbf{x})\,[\mathbf{n}(\mathbf{x}_0)\cdot\nabla G^{\mathrm{L}}(\mathbf{x},\mathbf{x}_0)] + [1-\mathbf{n}(\mathbf{x}_0)\cdot\mathbf{n}(\mathbf{x})]\,\frac{\partial G^{\mathrm{L}}}{\partial x_j}(\mathbf{x},\mathbf{x}_0)\,n_k(\mathbf{x}) - \frac{1}{8\pi}T_{ijk}(\mathbf{x},\mathbf{x}_0)\,[n_i(\mathbf{x})+n_i(\mathbf{x}_0)]\,n_k(\mathbf{x})\Big\}\,dS(\mathbf{x}). \tag{8.17}$$

In the case of the free-space Green's function, we recover expression (2.11) of Zinchenko *et al.* [211] obtained using a somewhat different method.

8.5. *Iterative Solution of the Integral Equations*

If all interfaces are closed, the integral equations of the second kind may be solved by the method of successive substitutions, as long as none of the fluids is inviscid. The rate of convergence may be improved by removing the marginal eigenvalues using the method of Weilandt deflation developed by Kim and Karrila [66] and discussed by Pozrikidis [127]. Zinchenko *et al.* [210] found that, even with eigenvalue removal, the rate of convergence becomes prohibitively slow when two interfaces are separated by a small distance, and implemented the method of biconjugate gradients as an alternative.

8.6. *Mesh-Control and Regridding*

In a typical numerical implementation, a three-dimensional interface is regarded as being composed of a continuous distribution of marker points that are labeled permanently using two "convected" surface curvilinear coordinates (ξ,η). If the positions of the marker points are described by the function $\mathbf{X}(\xi,\eta,t)$, then the motion of the marker points is governed by the differential equation defining the marker point velocity $\mathbf{U}=d\mathbf{X}/dt$, which is to be integrated in time subject to a specified initial condition. Kinematic considerations require that the normal component of the marker point velocity be equal to the normal component of the velocity of the fluid, but the tangential component may be arbitrary. The general form of the marker point velocity is given in Eq. (3.18).

The choice of the marker point velocity is exercised with the practical objective of preventing point clustering that may lead to numerical instabilities and deter the spatial resolution. For example, if an interface is stationary, it is appropriate to set the tangential marker point velocity to zero, $\mathbf{w}=\mathbf{0}$, so that the marker points remain stationary. When, on the other hand, the interface translates with velocity $\mathbf{U}^{\mathrm{TR}}$ without deformation, it is appropriate to set $\mathbf{w}=\mathbf{P}\cdot\mathbf{U}^{\mathrm{TR}}$ so that the marker points retain their relative position.

A dynamical simulation involves the computation of the motion of a finite collection of marker points defining the vertices of boundary elements. Loewenberg and Hinch [91, 92] and Cristini *et al.* [26] developed a method of dynamically adjusting the tangential velocity of the marker points over the interfaces of two interacting drops in simple shear flow. Coulliette and Pozrikidis [25] used a variation of their method to simulate the motion of a file of drops in Poiseuille flow. Zinchenko *et al.* [210, 211] and Zinchenko and Davis [209] found that an alternative method, "passive mesh stabilization," performs better for more

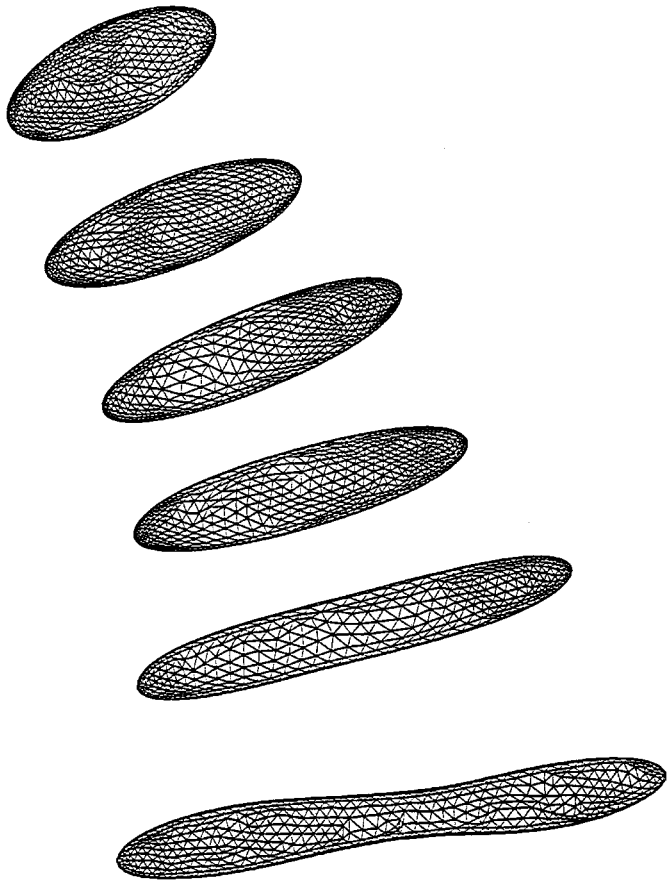

FIG. 6. Deformation of a low-viscosity liquid drop in infinite simple shear flow computed by the method of interfacial dynamics. Interfacial regridding is done with the advancing front method [72].

general types of motion. Their algorithm is based on the idea of computing the tangential velocity of each node by minimizing a carefully devised objective function defined with respect to the distances between nodes, the maximum mean curvature of the interface, and the element surface areas.

Kwak and Pozrikidis [72] implemented regridding in physical space using the advancing front method. The advantage of this approach is that the density of the interfacial elements may readily be increased or descreased at regions of high or low curvature, while the size of the triangles and their skewness is kept within specified thresholds, independent of the motion. Stages in the deformation of a low-viscosity liquid drop subject to an infinite simple shear flow simulated using this method are shown in Fig. 6.

8.7. *Smoothing*

Dynamical simulations of interfacial motion suffer from numerical instabilities whose severity depends on the type of flow and physical properties of the interface. Since interfacial dynamics in Stokes flow is inherently well posed, as opposed to vortex-sheet dynamics in inviscid flow, which is inherently ill posed, the instabilities may be eliminated by improving the accuracy of the numerical method, by decreasing the size of the time step, or by doing

both. In practice, however, the higher the spatial resolution, the smaller the time step for a stable simulation, and this inflates the cost of the simulation. A practical alternative for carrying out extended simulations is to filter out numerical oscillations by smoothing the position of marker points and possibly dynamically active fields over the interfaces. Smoothing may be interpreted in two complementary ways: local or global polynomial or Fourier spectrum expansion followed by truncation; and the implementation of an evolution law for the smoothed function incorporating second- or fourth-order diffusion.

Smoothing two-dimensional and axisymmetric shapes and functions defined over them can be done efficiently using formulae derived by Longuet–Higgins and Cokelet [94] and Dold [34]. Numerical methods for smoothing three-dimensional shapes described by triangulation are less well developed. Zinchenko *et al.* [211] and Zinchenko and Davis [209] eliminated surface irregularities by adding to the normal component of the velocity an additional term involving the local mean curvature or the surface Laplacian of the third power of the mean curvature. Pozrikidis [143] implemented smoothing by mapping a closed interface onto the unit sphere, expanding the smoothed function in surface harmonics defined in terms of associated Legendre functions, truncating the spectrum of the expansion, and then reproducing the surface function from the truncated expansion.

8.8. *Spectral-Element Methods*

Occhialini *et al.* [116], Muldowney and Higdon [109], and Pozrikidis [141] implemented spectral-element orthogonal-collocation methods for solving the integral equations of two- and three-dimensional Stokes flow. In the case of three-dimensional flow considered by Higdon and coworkers, the elements have rectangular shapes.

Basis functions for spectral expansions over triangular elements defined in terms of Jacobi polynomials have been developed by Dubiner [35] and Sherwin and Karniadakis [165], as discussed by Heinrichs [57]. In the orthogonal collocation method, the integral equation is enforced at scaled zeros of the basis functions or scaled base points of a Gauss-triangle integration quadrature to achieve spectral accuracy. The accurate computation of the singular boundary integrals, however, requires the use of specialized quadratures for numerical integration of singular, weakly singular, and nearly singular integrals over surface elements that are not available.

8.9. *Fast-Summation Methods*

When a large number of interfaces are involved, the computation of the single- and double-layer hydrodynamic potential becomes prohibitively expensive, and the use of expedited or fast summation methods for solving the integral equations becomes necessary. In one approach, the number of function evaluations is reduced by expressing the interaction between two well-separated particles in terms of multipole expansions, where the coefficients of the singularities are computed from the instantaneous geometrical shapes [22]. In the fast-multipole-method for Stokes flow developed by Sangani and Mo [158] for suspensions of spherical particles, the Stokes-flow singularities are grouped into boxes, and their induced velocity is expressed in terms of multipole expansions. Zinchenko and Davis [209] argued that an alternative approach is better suited for nonspherical interfaces in triply periodic flow. The development and implementation of efficient general-purpose fast-solution methods is an area of active research [70].

TABLE I

Categories of Problems Studied by the Method of Interfacial Dynamics for Stokes Flow. The Qualifiers 3D, 2D, and Axs, Stand, Respectively, for Three-Dimensional, Two-Dimensional, and Axisymmetric Flow

Drops and bubbles

- Deformation of a drop or bubble in extensional flow (2D, axs): Youngren and Acrivos [201], Rallison and Acrivos [149], Pozrikidis [134, 137].
- Relaxation of an extended drop (axs): Stone and Leal [177, 178], Tjahjadi *et al.* [185], Lister and Stone [90].
- Deformation of a compund drop or liquid shell in extensional flow (axs): Stone and Leal [179].
- Deformation of a drop in infinite linear flow (3D): Rallison [148], Kennedy *et al.* [65], Uijttewaal and Nijhof [189], Kwak and Pozrikidis [72].
- Motion of a rising or falling drop (axs): Koh and Leal [68], Pozrikidis [124], Muldowney and Higdon [109].
- Deformation of a drop in a rotating fluid (axs): Lister and Stone [89].
- Deformation of an electrically charged drop (axs): Baygents *et al.* [13].

Drop and bubble interactions

- Interaction of rising or falling drops (axs, 3D): Manga and Stone [98, 99, 100], Manga [97], Davis [29], Zinchenko *et al.* [211], Roumeliotis and Fulford [155].
- Pairwise drop interception in shear flow (2D, 3D): Loewenberg and Hinch [92], Li and Pozrikidis [109].

Periodic suspensions

- Simple shear flow of doubly-periodic suspensions (2D): Li *et al.* [81], Charles and Pozrikidis [22].
- Simple shear flow of triply-periodic suspensions (3D): Pozrikidis [129], Loewenberg and Hinch (1996) [91], Loewenberg [93], Zinchenko and Davis [209].

Drops and bubbles near walls and interfaces

- Motion of a drop normal to an interface (axs): Chi and Leal [23], Ascoli *et al.* [3], Tanzosh *et al.* [184], Koch and Koch [67].
- Gravity-driven motion of a drop normal to a wall (axs): Pozrikidis [125].
- Drop in shear flow above a plane wall (3D): Uijtterwaal *et al.* [188], Kennedy *et al.* [65], Uijtterwaal and Nijhof [189].

Flow past drops and bubbles adhering to a wall

- Shear flow past a drop adhering to a wall (2D, 3D): Li and Pozrikidis [82], Dimitrakopoulos and Higdon [31, 32], Yon and Pozrikidis [199], Schleizer and Bonnecaze [160].

Drops and bubbles in tube and channel flows

- Drops moving through a circular tube due to pressure gradient or gravity (axs): Martinez and Udell [102, 103], Pozrikidis [128].
- Suspensions of drops in plane Couette/Poiseuille or semi-infinite shear flow above a plane wall (2D): Zhou and Pozrikidis [205, 206, 207], Halpern *et al.* [50], Li and Pozrikidis [84].
- Semi-infinite bubble through a compliant channel with elastic walls (2D): Gaver *et al.* [44], Yap and Gaver [197].
- Motion of drops through a branched or converging-diverging channel (2D): Manga [95], Khayat *et al.* [63].
- Droplet motion in a cavity (2D): Manga [96].
- Motion of a file of drops through a circular tube (3D): Coulliette and Pozrikidis [25].

Drop at the tip of a tube

- Drop or bubble at the tip of a tube (axs): Zhang and Stone [203], Wong *et al.* [195].

Drops and bubbles in the presence of surfactants

- Self-induced deformation of a capsule (axs): Sapir and Nir [159].
- Drop in elongational flow (2D, axs): Stone and Leal [180], Milliken *et al.* [106], Pawar and Stebe [118], Pozrikidis [137], Eggleton and Stebe [39], Eggleton *et al.* [38].
- Deformation of a drop translating in infinite space or through a tube (axs): Borhan and Mao [16], Tsai and Miksis [187], Johnson and Borhan [60, 61].
- Deformation of a drop in linear flow (3D): Li and Pozrikidis [83], Yon and Pozrikidis [198].

TABLE I—*Continued*

- Deformation of a drop adhering to a wall (2D, 3D): Yon and Pozrikidis [199], Schleizer and Bonnecaze [160].
- Bubble at the tip of a tube (axs): Wong *et al.* [196].
- Semi-infinite bubble through a flexible channel (2D): Yap and Gaver [197].

Thermocapillary motion

- Motion of a drop near a plane wall (axs): Ascoli and Leal [4].
- Migration of two deformable drops (axs): Zhou and Davis [204].

Drop and bubble coalescence and sintering

- Coalescence of two drops (2D, axs): Hiram and Nir [58], Kuiken [71], Primo *et al.* [147].
- Shrinkage of bubbles trapped in a liquid (2D, axs): Van de Vorst [190, 191, 192], Primo *et al.* [146].

Liquid threads and annular layers

- Instability of threads and annular layers coated on the interior surface of a circular tube (axs): Newhouse and Pozrikidis [114], Pozrikidis [140], Kwak and Pozrikidis [73], Kwak *et al.* [75].
- Instability of a liquid bridge subtended between two coaxial cylinders (axs): Gaudet *et al.* [43, 44].

Liquid capsules

- Capsules with fibrous interfaces (axs): Sapir and Nir [159], Nir [115], Zinemanas and Nir [212, 213, 214].
- Elastic capsules in elongational flow (axs): Li *et al.* [80], Bathès–Biesel [9], Diaz *et al.* [30], Kwak and Pozrikidis [74].
- Elastic capsules passing through constrictions (axs): Leyrat–Maurin and Barthès–Biesel [79].
- Capsules with viscous interfaces (3D): Pozrikidis [130].
- Capsules with incompressible interfaces (axs, 3D): Pozrikidis [126], Zhou and Pozrikidis [208], Kraus *et al.* [69].
- Elastic capsules with various unstressed shapes in simple shear flow (3D): Pozrikidis [131], Ramanujan and Pozrikidis [150], Navot [112], Pozrikidis [109].
- Deformation of elastic capsules and flow of doubly-periodic suspensions (2D): Breyiannis and Pozrikidis [18].

Films, layers, and extended interfaces

- Extruded film flow (2D): Kelmanson [62].
- Film flow down a plane wall into a pool (2D): Hansen [52].
- Film-flow down a periodic wall (2D): Pozrikidis [123].
- Deformation of an interface due to liquid withdrawal (axs): Lister [87].
- Spreading of a liquid over an interface (2D, axs): Lister and Kerr [88].
- Gravitational instability of a film on a plane wall (2D): Newhouse and Pozrikidis [113].
- Film-flow down a plane wall with a hump or an attached particle (2D, 3D): Hansen [51, 53], Pozrikidis and Thoroddsen [145].
- Multilayer flows (2D): Pozrikidis [134, 135, 138].

Rigid particles near interfaces

- Motion of spherical particles normal to a deformable interface (axs): Leal and Lee [77], Lee and Leal [78], Geller *et al.* [46], Stoos and Leal [181, 182], Manga and Stone [100].

9. OVERVIEW OF APPLICATIONS

Several versions of the method of interfacial dynamics for Stokes flow have been implemented to study a variety of problems in science and engineering with applications in materials science, chemical engineering, geophysics, and biomechanics. A review of early work was given by Tanzosh *et al.* [184] and Stone [176]. Table I presents an overview of flow configurations considered, illustrating the diversity of the applications and summarizing the state of the art regarding theoretical development and numerical implementation. The abbreviations 3D, 2D, and axs stand, respectively, for three-dimensional, two-dimensional, and axisymmetric flow. A collection of simulation programs that solve several families of problems is available in the fluid dynamics library FDLIB [139].

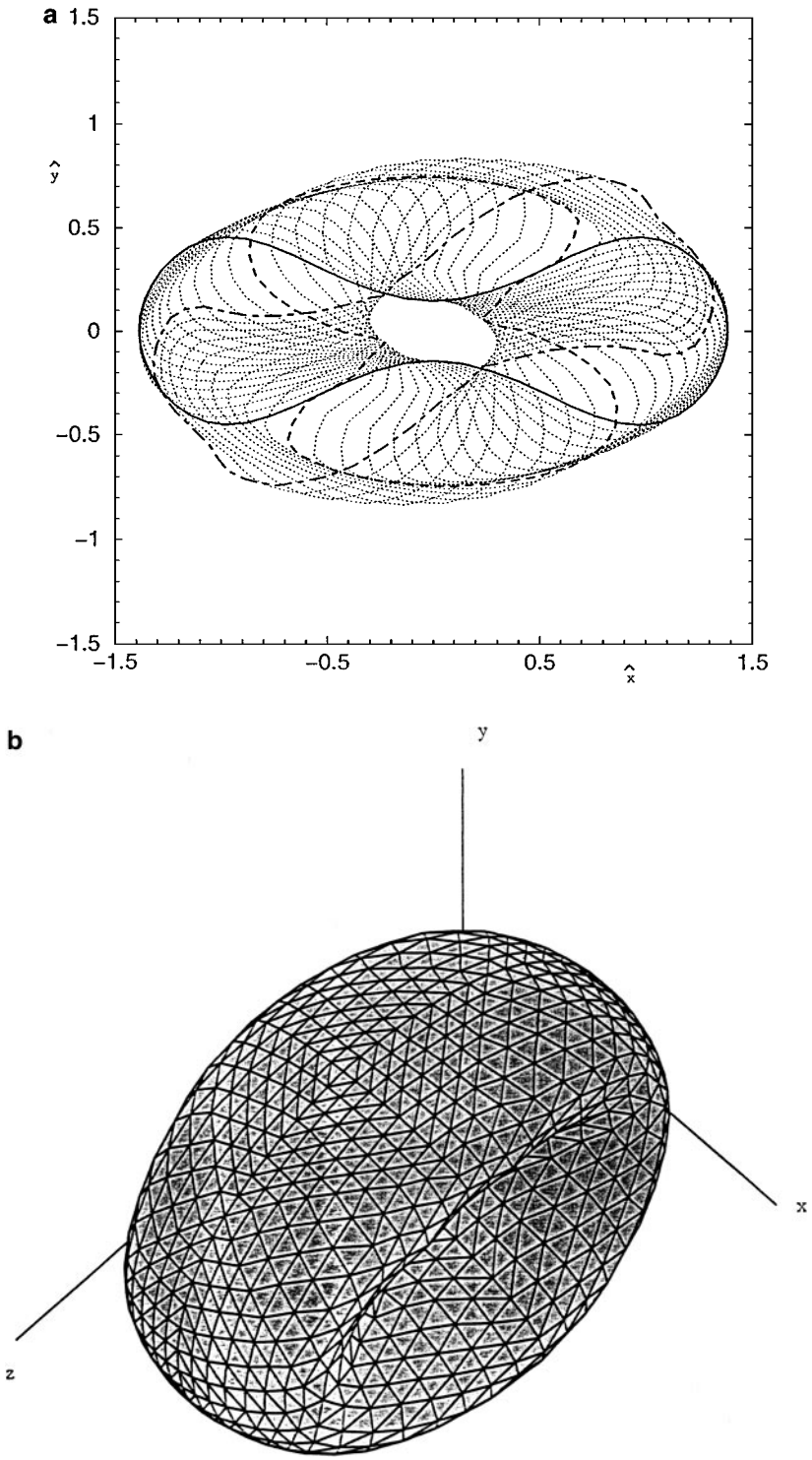

FIG. 7. Deformation of a liquid capsule enclosed by an elastic membrane whose unstressed shape is a biconcave disk, subject to simple shear flow along the x axis [144]. (a) Sequence of profiles in the xy plane of symmetry; the heavy solid line corresponds to the biconcanve disk; (b, c) three-dimensional perspectives corresponding to the shapes drawn with the heavy dashed lines in (a).

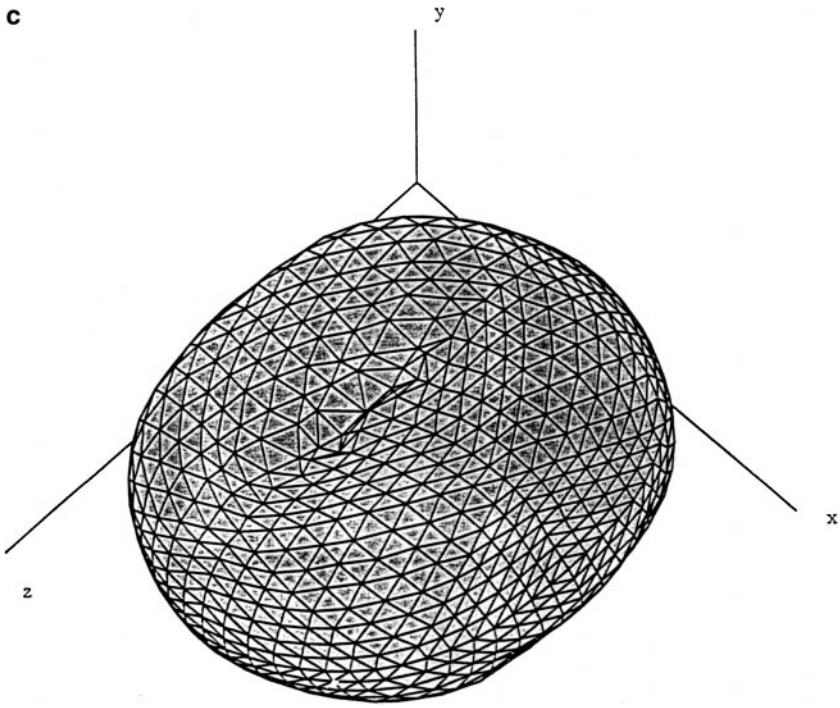

FIG. 7—*Continued*

We conclude this section by presenting two illustrations. Figure 7 shows results of recent simulations on the deformation of a liquid capsule enclosed by an elastic membrane with the unstressed shape of a biconcave disk, subject to a simple shear flow [144]. Figure 7a illustrates a sequence of profiles in the plane of symmetry, with the heavy solid line corresponding to the biconcanve disk, and Figs. 7b–7c illustrate three-dimensional perspectives corresponding to the profiles drawn with the heavy dashed lines in Fig. 7a. Figure 8 shows instantaneous profiles of liquid drops in a two-dimensional doubly periodic suspension evolving under the influence of a simple shear flow; the interfaces are occupied by an insoluble surfactant (simulation conducted for the purpose of this review).

10. FUTURE DEVELOPMENTS

Since the pioneering work of Youngren and Acrivos [201], some 25 years ago, considerable progress has been made in the theoretical foundation and implementation of boundary-integral methods for interfacial flow. The general subject continues to attract the attention of researchers in the fields of applied mathematics, computational science, and mainstream engineering, and short courses are offered in at least two institutions. In the preceding sections, we identified several topics for further theoretical and computational development, including the following:

- Investigation of the properties of the integral equations for suspensions of drops and capsules with different physical properties and general flow configurations.
- Development of fast methods for the iterative solution of the integral equations.
- Development of efficient integration quadratures for singular integrands over three-dimensional elements with flat and curved shapes.

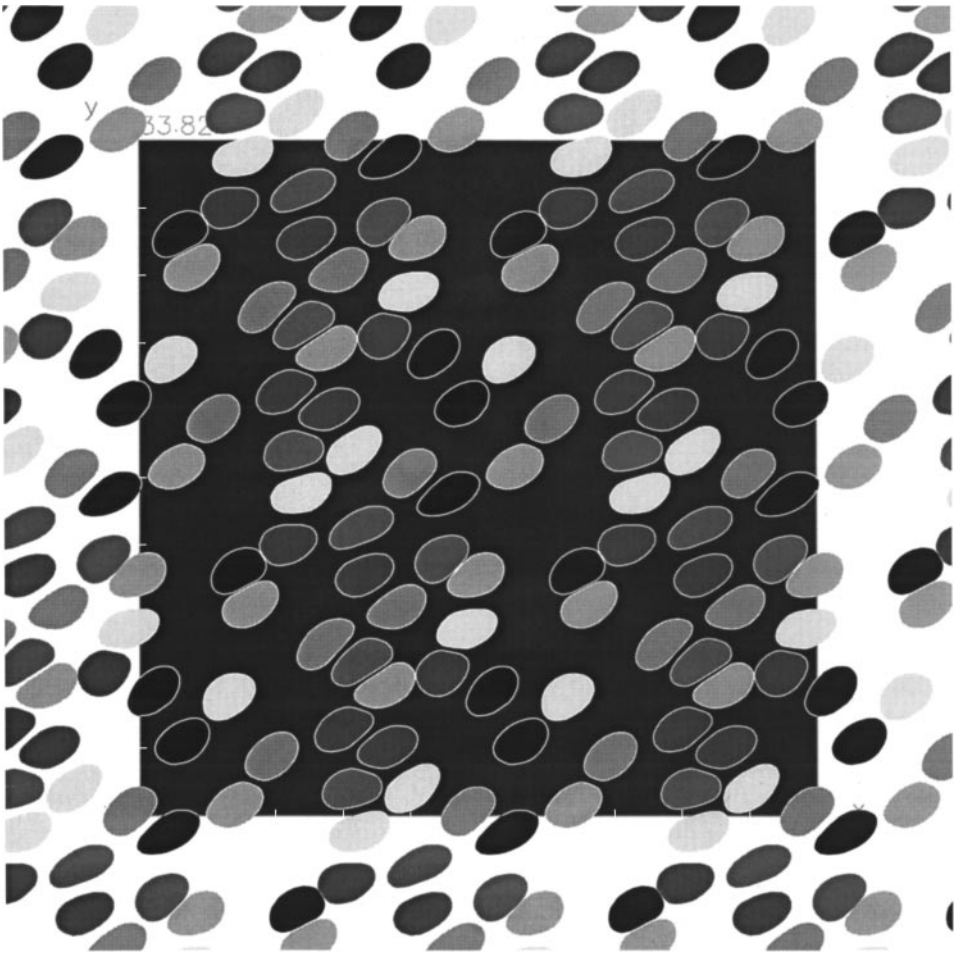

FIG. 8. Instantaneous profiles of liquid drops in a two-dimensional doubly-periodic suspension evolving under the influence of a simple shear flow in the horizontal direction; the interfaces are occupied by an insoluble surfactant.

- Implementation of spectral-element methods over triangulated interfaces.
- Numerical methods for smoothing the position of interfacial marker points and functions defined over a three-dimensional interfaces.
- Fast, general-purpose methods for simulating large systems in two- and three-dimensional flow.
- Development of robust algorithms for regridding in triangulaton.
- Development of efficient formulations for nonNewtonian fluids and flow at nonzero Reynolds number.

Among all fields of application, the field of biomechanics and biorheology is likely to benefit the most from the efficiency, elegance, and convenience of the method of interfacial dynamics for Stokes flow. The next decade is expected to witness the growth of the emerging discipline of computational biomechanics, and boundary-integral methods, and those who contribute to their development and implementation, will certainly play an important role.

APPENDIX

Consider a nonsingular vector function **F** defined in three-dimensional space, and an open surface D bounded by the closed contour C. Stokes' circulation theorem provides us with the identity

$$\int_D (\nabla \times \mathbf{F}) \cdot \mathbf{n}\, dS = \int_C \mathbf{F} \cdot \mathbf{t}\, dl, \tag{A.1}$$

where **n** is the unit vector normal to D, **t** is the unit vector tangential to C oriented according to the right-handed rule with respect to **n**, and l is the arc length along C measured in the direction of **t**. Setting $\mathbf{F} = \mathbf{A} \times \mathbf{B}$, where **A** and **B** are two arbitrary nonsingular vector functions defined in the three-dimensional space, and reverting to index notation, we find

$$\epsilon_{ijk}\epsilon_{klm} \int_D \frac{\partial}{\partial x_j}(A_l B_m) n_i\, dS = \int_C F_i t_i\, dl. \tag{A.2}$$

Straightforward manipulation of the left-hand side of (A.2) yields

$$\begin{aligned}(\delta_{il}\delta_{jm} - \delta_{im}\delta_{jl}) &\int_D \frac{\partial}{\partial x_j}(A_l B_m) n_i\, dS \\ &= \int_D \frac{\partial}{\partial x_j}(A_i B_j) n_i\, dS - \int_D \frac{\partial}{\partial x_j}(A_j B_i) n_i\, dS = \int_C F_i t_i\, dl.\end{aligned} \tag{A.3}$$

If the surface D is closed, the integral on the right-hand side of (A.3) vanishes yielding the identity

$$\int_D \frac{\partial}{\partial x_j}(A_i B_j) n_i\, dS = \int_D \frac{\partial}{\partial x_j}(A_j B_i) n_i\, dS. \tag{A.4}$$

As an application, we identify the vector function **A** with one of the unit vectors (1, 0, 0), (0, 1, 0), or (0, 0, 1), and obtain the identity

$$\int_D \frac{\partial B_j}{\partial x_j} n_i\, dS = \int_D \frac{\partial B_j}{\partial x_i} n_j\, dS \tag{A.5}$$

presented by Rosenkilde [156].

ACKNOWLEDGMENTS

Andrea Brunson helped with the preparation of the manuscript. This work has been supported by a grant provided by the National Science Foundation.

REFERENCES

1. A. W. Adamson, *Physical Chemistry of Surfaces*, 5th ed. (Wiley, New York, 1990).
2. D. M. Anderson, G. B. McFadden, and A. A. Wheeler, Diffuse-interface methods in fluid mechanics, *Annu. Rev. Fluid Mech.* **30**, 139 (1988).
3. E. P. Ascoli, D. S. Dandy, and L. G. Leal, Buoyancy-driven motion of a deformable drop toward a planar wall at low Reynolds number, *J. Fluid Mech.* **213**, 287 (1990).
4. E. P. Ascoli and L. G. Leal, Thermocapillary motion of a deformable drop toward a plane wall, *J. Colloid Interface Sci.* **138**, 220 (1992).

5. R. Aris, *Vectors, Tensors and the Basic Equations of Fluid Mechanics* (Prentice–Hall, Englewood Cliffs, NJ, 1962).
6. G. R. Baker, *Generalized Vortex Method for Free-Surface Flows in Waves and Fluid Interfaces*, (MRC, University of Wisconsin, 1983).
7. G. R. Baker, D. I. Meiron, and S. A. Orszag, Boundary integral methods for axisymmetric and three-dimensional Rayleigh–Taylor instability problems, *Physica D* **12**, 19 (1984).
8. D. Barthès-Biesel, Motion of a spherical microcapsule freely suspended in a linear shear flow, *J. Fluid Mech.* **100**, 831 (1980).
9. D. Barthès-Biesel, Role of interfacial properties on the motion and deformation of capsules in shear flow, *Physica A* **172**, 103 (1991).
10. D. Barthès-Biesel and H. Sgaier, Role of membrane viscosity in the orientation and deformation of a spherical capsule suspended in shear flow, *J. Fluid Mech.* **160**, 119 (1985).
11. D. Barthès-Biesel and J. M. Rallison, The time-dependent deformation of a capsule freely suspended in a linear shear flow, *J. Fluid Mech.* **113**, 251 (1981).
12. G. K. Batchelor, The stress system in a suspension of force-free particles, *J. Fluid Mech.* **41**, 545 (1970).
13. J. C. Baygents, N. J. Rivette, and H. A. Stone, Electrohydrodynamic deformation and interaction of drop pairs in viscous fluids, *J. Fluid Mech.* **368**, 359 (1998).
14. M. F. Beatty, Topics of finite elasticity: Hyperelasticity of rubber, elastomers and biological tissues—with examples, *Appl. Mech. Rev.* **40**, 1699 (1987).
15. S. K. Boey, D. H. Boal, and D. E. Discher, Simulations of the erythrocyte cytoskeleton at large deformation. I. Microscopic models, *Biophys. J.* **75**, 1573 (1998).
16. A. Borhan and C. F. Mao, Effect of surfactants on the motion of drops through circular tubes, *Phys. Fluids A* **4**, 2628 (1992).
17. C. A. Brebbia, *The Boundary Element Method for Engineers* (Pentech Press, London, 1978).
18. G. Breyiannis and C. Pozrikidis, Simple shear flow of suspensions of elastic capsules, *Theor. Comput. Fluid Dyn.* **13**, 327 (2000).
19. B. Budiansky, Notes on nonlinear shell theory, *J. Applied Mech.* **35**, 393 (1968).
20. B. Budiansky and J. L. Sanders, Jr., On the "best" first-order linear shell theory, in *Progress in Applied Mechanics, Prager University Volume* (McMillan, New York, 1963), p. 129.
21. W. Cai and T. C. Lubensky, Hydrodynamics and dynamic fluctuations of fluid membranes, *Phys. Rev. E* **52**, 4252 (1995).
22. R. Charles and C. Pozrikidis, Significance of the dispersed-phase viscosity on the simple shear flow of suspensions of two-dimensional liquid drops, *J. Fluid Mech.* **365**, 205 (1998).
23. B. K. Chi and L. G. Leal, A theoretical study of the motion of a viscous drop toward a fluid interface at low Reynolds number, *J. Fluid Mech.* **201**, 123 (1989).
24. A. H. Corneliussen and R. T. Shield, Finite deformation of elastic membranes with application to the stability of an inflated and extended tube, *Arch. Rational Mech. Anal.* **7**, 273 (1961).
25. C. Coulliette and C. Pozrikidis, Motion of liquid drops through tube, *J. Fluid Mech.* **358**, 1 (1988).
26. V. Cristini, J. Blawzdziewicz, and M. Loewenberg, Drop breakup in three-dimensional viscous flows, *Phys. Fluids* **10**, 1781 (1998).
27. K. Davey and S. Hinduja, Analytical integration of linear three-dimensional triangular elements in BEM, *Appl. Math. Modeling* **13**, 450 (1989).
28. A. M. J. Davis, Force and torque formulae for a sphere moving in an axisymmetric stokes flow with finite boundaries: Asymmetric stokeslets near a hole in a plane wall, *Int. J. Multiphase Flow* **9**, 575 (1983).
29. R. H. Davis, Buoyancy-driven viscous interaction of a rising drop with a smaller trailing drop, *Phys. Fluids* **11**, 1016 (1999).
30. A. Diaz, N. Pelekasis, and D. Barthès-Biesel, Transient response of a capsule subjected to varying flow conditions: Effect of internal fluid viscosity and membrane elasticity, *Phys. Fluids* **12**, 948 (2000).
31. P. Dimitrakopoulos and J. J. L. Higdon, Displacement of fluid droplets from solid surfaces in low-Reynolds-number shear flows, *J. Fluid Mech.* **336**, 351 (1997).

32. P. Dimitrakopoulos and J. J. L. Higdon, On the displacement of three-dimensional fluid droplets from solid surfaces in low-Reynolds-number shear flows, *J. Fluid Mech.* **377**, 189 (1998).
33. D. E. Discher, D. H. Boal, and S. K. Boey, Simulations of the erythrocyte cytoskeleton at large deformation. II. Micropipette aspiration, *Biophys. J.* **75**, 1584 (1998).
34. J. W. Dold, An efficient surface-integral algorithm applied to unsteady gravity waves, *J. Comput. Phys.* **103**, 90 (1992).
35. M. Dubiner, Spectral methods on triangles and other domains, *J. Sci. Comput.* **6**, 345 (1991).
36. D. A. Edwards, H. Brenner, and D. T. Wasan, *Interfacial Transport Processes and Rheology* (Butterworth Heinemann, Massachusetts, 1991).
37. C. D. Eggleton and A. S. Popel, Large deformation of red blood cell ghosts in a simple shear flow, *Phys. Fluids* **10**, 1834 (1998).
38. C. D. Eggleton, W. P. Pawar, and K. J. Stebe, Insoluble surfactants on a drop in an extensional flow: A generalization of the stagnated surface limit to deforming interfaces, *J. Fluid Mech.* **385**, 79 (1999).
39. C. D. Eggleton and K. B. Stebe, An adsorption–desorption-controlled surfactant on a deforming droplet, *J. Colloid Interf. Sci.* **208**, 68 (1998).
40. E. A. Evans and R. Skalak, *Mechanics and Thermodynamics of Biomembranes* (CRC Press, Boca Raton, FL, 1980).
41. W. Flügge, *Stresses in Shells* (Springer–Verlag, Berlin, 1973).
42. Y. C. Fung, *Foundations of Solid Mechanics* (Prentice–Hall, Englewood Cliffs, NJ, 1965).
43. S. Gaudet, G. H. McKinley, and H. A. Stone, Extensional deformation of Newtonian and non-Newtonian liquid bridges in microgravity, AIAA-94-0696, presented at 32nd Aerospace Sciences Meeting and Exhibit (1994).
44. S. Gaudet, G. H. McKinley, and H. A. Stone, Extensional deformation of liquid bridges, *Phys. Fluids A* **8**, 2568 (1996).
45. D. P. Gaver III, D. Halpern, O. E. Jensen, and J. B. Grotberg, The steady motion of a semi-infinite bubble through flexible-walled channel, *J. Fluid Mech.* **319**, 25 (1986).
46. A. S. Geller, S. H. Lee, and L. G. Leal, The creeping motion of a spherical particle normal to a deformable interface, *J. Fluid Mech.* **169**, 27 (1986).
47. A. E. Green and J. E. Adkins, *Large Elastic Deformations* (Clarendon, Oxford, 1970).
48. A. E. Green and W. Zerna, *Theoretical Elasticity* (Dover, New York, 1968).
49. M. E. Gurtin and A. I. Murdoch, A continuum theory of elastic material surfaces, *Arch. Ration. Mech. Anal.* **57**, 291 (1975).
50. D. Halpern, Y. Jiang, and J. F. Himm, Mathematical model of gas bubble evolution in a straight tube, *J. Biomed. Eng.* **121**, 505 (1999).
51. E. B. Hansen, Free surface Stokes flow over an obstacle, in *Boundary Elements VIII Conference* (1986), p. 783.
52. E. B. Hansen, Stokes flow down a wall into an infinite pool, *J. Fluid Mech.* **178**, 243 (1987).
53. E. B. Hansen, Stokes flow of a fluid layer over an obstacle on a tilted plane, *Math. Comput. Modelling* **15**, 185 (1991).
54. J. C. Hansen, R. Skalak, S. Chien, and A. Hoger, An elastic network model based on the structure of the red blood cell membrane skeleton, *Biophys. J.* **70**, 146 (1996).
55. J. C. Hansen, R. Skalak, S. Chien, and A. Hoger, Influence of network topology on the elasticity of the red blood cell membrane skeleton, *Biophys. J.* **72**, 2369 (1997).
56. J. C. Hansen, R. Skalak, S. Chien, and A. Hoger, Spectrin properties and the elasticity of the red blood cell membrane skeleton, *Biorheology* **34**, 327 (1997).
57. W. Heinrichs, Spectral collocation on triangular elements, *J. Comput. Phys.* **145**, 743 (1998).
58. Y. Hiram and A. Nir, A simulation of surface tension driven coalescence, *J. Colloid Interface Sci.* **95**, 462 (1983).

59. M. A. Jawson, Integral equation methods in potential theory, I, *Proc. R. Soc. A* **275**, 23 (1963).

60. R. A. Johnson and A. Borhan, Effect of insoluble surfactants on the pressure-driven motion of a drop in a tube in the limit of high surface coverage, *J. Colloid Interface Sci.* **218**, 184 (1999).

61. R. A. Johnson and A. Borhan, Stability of the shape of a surfactant-laden drop translating at low Reynolds number, *Phys. Fluids* **12**, 773 (2000).

62. M. A. Kelmanson, Boundary integral equation solution of viscous flows with free surfaces, *J. Eng. Math.* **17**, 329 (1983).

63. R. E. Khayat, A boundary element analysis of multiply-connected three-dimensional cavity mixing flow of polymer solutions, *Int. J. Num. Meth. Fluids* **31**, 1173 (1999).

64. R. E. Khayat, A. Luciani, L. A. Utracki, F. Godbille, and J. Picot, Influence of shear and elongation on drop deformation in convergent–divergent flows, *Int. J. Multiphase Flow* **26**, 17 (2000).

65. M. R. Kennedy, C. Pozrikidis, and R. Skalak, Motion and deformation of liquid drops and the rheology of dilute emulsions in simple flow, *Comput. Fluids* **23**, 251 (1994).

66. S. Kim and S. J. Karrila, *Microhydrodynamics: Principles and Selected Applications* (Butterworth Heinemann, Massachusetts, 1991).

67. D. M. Koch and D. L. Koch, Numerical and theoretical solutions for a drop spreading below a free fluid surface, *J. Fluid Mech.* **287**, 251 (1995).

68. C. J. Koh and L. G. Leal, The stability of drop shapes for translation at zero Reynolds number through a quiescent fluid, *Phys. Fluids A* **1**, 1309 (1989).

69. M. Kraus, W. Wintz, U. Seifert, and R. Lipowsky, Fluid vesicles in shear flow, *Phys. Rev. Lett.* **77**, 3685 (1996).

70. M. C. A. Kropinski, Integral equation methods for particle simulations in creeping flows, *Comput. Math. Appl.* **38**, 67 (1999).

71. H. K. Kuiken, Viscous sintering: The surface-tension-driven flow of a liquid form under the influence of curvature gradients at its surface, *J. Fluid Mech.* **214**, 503 (1990).

72. S. Kwak and C. Pozrikidis, Adaptive triangulation of evolving, closed or open surfaces by the advancing-front method, *J. Comput. Phys.* **145**, 61 (1998).

73. S. Kwak and C. Pozrikidis, Effect of surfactants on the instability of a liquid thread or an annular layer. 1. Quiescent fluids, *Int. J. Multiphase Flow*, in press (2000).

74. S. Kwak and C. Pozrikidis, Effect of flexural stiffness on the deformation of capsules in uniaxial extensional flow, submitted for publication (2000).

75. S. Kwak, M. M. Firyllas, and C. Pozrikidis, Effect of surfactants on the instability of a liquid thread. 2. Extensional flow, *Int. J. Multiphase Flow*, in press (2000).

76. H. LeDret and A. Raoult, The nonlinear membrane model as variational limit of nonlinear three-dimensional elasticity, *J. Math. Pures Appl.* **74**, 549 (1995).

77. L. G. Leal and S. H. Lee, Particle motion near a deformable fluid interface, *Adv. Colloid Interface Sci.* **17**, 61 (1982).

78. S. H. Lee and L. G. Leal, The motion of a sphere in the presence of a deformable interface. II. A numerical study of the translation of a sphere normal to an interface, *J. Colloid Interface Sci.* **87**, 81 (1982).

79. A. Leyrat-Maurin and D. Barthès-Biesel, Motion of a deformable capsule through a hyperbolic constriction, *J. Fluid Mech.* **279**, 135 (1994).

80. X. Z. Li, D. Barthès-Biesel, and A. Helmy, Large deformations and burst of a capsule freely suspended in elongational flow, *J. Fluid Mech.* **187**, 179 (1988).

81. X. Li, R. Charles, and C. Pozrikidis, Simple shear flow of suspensions of liquid drops, *J. Fluid Mech.* **320**, 395 (1996).

82. X. Li and C. Pozrikidis, Shear flow over a liquid drop adhering to a solid surface, *J. Fluid Mech.* **307**, 167 (1996).

83. X. Li and C. Pozrikidis, Effect of surfactants on drop deformation and on the rheology of dilute emulsions in Stokes flow, *J. Fluid Mech.* **341**, 165 (1997).

84. X. Li and C. Pozrikidis, Wall-bounded and channel flow of suspensions of liquid drops, *Int. J. Multiphase Flow* **26**, 1247 (2000).

85. A. Libai and J. G. Simmonds, *The Nonlinear Theory of Elastic Shells* (Cambridge Univ. Press, Cambridge, UK, 1998).
86. R. Lipowsky, The conformation of membranes, *Nature* **349**, 475 (1991).
87. J. R. Lister, Selective withdrawal from a viscous two-layer system, *J. Fluid Mech.* **198**, 231 (1989).
88. J. R. Lister and R. C. Kerr, The propagation of two-dimensional and axisymmetric viscous gravity currents at a fluid interface, *J. Fluid Mech.* **203**, 215 (1989).
89. J. R. Lister and H. A. Stone, Time-dependent viscous deformation of a drop in a rapidly rotating denser fluid, *J. Fluid Mech.* **317**, 275 (1996).
90. J. R. Lister and H. A. Stone, Capillary breakup of a viscous thread surrounded by another viscous fluid, *Phys. Fluids* **11**, 2758 (1998).
91. M. Loewenberg and E. J. Hinch, Numerical simulation of a concentrated emulsion in shear flow, *J. Fluid Mech.* **321**, 395 (1996).
92. M. Loewenberg and E. J. Hinch, Collision of two deformable drops in shear flow, *J. Fluid Mech.* **338**, 299 (1997).
93. M. Loewenberg, Numerical simulation of concentrated emulsion flows, *J. Fluid Eng.* **120**, 824 (1998).
94. M. S. Longuet–Higgins and E. D. Cokelet, The deformation of steep surface waves on water, I. A numerical method of computation, *Proc. Roy. Soc. London A* **350**, 1 (1976).
95. M. Manga, Dynamics of drops in branched tubes, *J. Fluid Mech.* **315**, 105 (1996).
96. M. Manga, Dynamics of drops in cavity flows: Aggregation of high viscosity ratio drops, *Phys. Fluids* **8**, 1732 (1996).
97. M. Manga, Interactions between mantle diapirs, *Geophys. Res. Lett.* **24**, 1871 (1997).
98. M. Manga and H. A. Stone, Buoyancy-driven interactions between the deformable viscous drops, *J. Fluid Mech.* **256**, 647 (1993).
99. M. Manga and H. A. Stone, Interactions between bubbles in magmas and lavas: Effects of deformation, *J. Volcanology Geothermal Res.* **63**, 269 (1994).
100. M. Manga and H. A. Stone, Low Reynolds number motion of bubbles, drops and rigid spheres through fluid–fluid interfaces, *J. Fluid Mech.* **287**, 279 (1995).
101. M. Manga and H. A. Stone, Collective hydrodynamics of deformable drops and bubbles in dilute low Reynolds number suspensions, *J. Fluid Mech.* **300**, 231 (1995).
102. M. J. Martinez and K. S. Udell, Boundary-integral analysis of the creeping flow of long bubbles in capillaries, *J. Appl. Mech.* **56**, 211 (1989).
103. M. J. Martinez and K. S. Udell, Axisymmetric creeping motion of drops through circular tubes, *J. Fluid Mech.* **210**, 565 (1990).
104. C. Maul and S. Kim, Image systems for a Stokeslet inside a rigid spherical container, *Phys. Fluids* **6**, 2221 (1994).
105. P. McDonald, *Continuum Mechanics* (PWS, Boston, 1996).
106. W. J. Milliken, H. A. Stone, and L. G. Leal, The effect of surfactant on the transient motion of Newtonian drops, *Phys. Fluids A* **5**, 69 (1993).
107. N. Mohandas and E. Evans, Mechanical properties of the red cell membrane in relation to molecular structure and genetic defect, *Annu. Rev. Biophys. Biomol. Struct.* **23**, 787 (1994).
108. H. Møllmann, *Introduction to the Theory of Thin Shells* (Wiley, New York, 1981).
109. G. P. Muldowney and J. J. L. Higdon, A spectral boundary element approach to three-dimensional Stokes flow, *J. Fluid Mech.* **298**, 167 (1995).
110. A. Nadim, A concise introduction to surface rheology with applications to dilute emulsions of viscous drops, *Chem. Eng. Commun.* **148–150**, 391 (1996).
111. P. M. Naghdi, Theory of shells and plates, in *Handbuch der Physik*, edited by C. Truesdell (1972), Vol. V1a, p. 435.
112. Y. Navot, Elastic membranes in viscous shear flow, *Phys. Fluids* **10**, 1819 (1998).
113. L. A. Newhouse and C. Pozrikidis, The Rayleigh–Taylor instability of a liquid layer resting on a plane wall, *J. Fluid Mech.* **217**, 615 (1990).

114. L. A. Newhouse and C. Pozrikidis, The capillary instability of annular layers and liquid threads, *J. Fluid Mech.* **242**, 193 (1992).

115. A. Nir, Deformation of some biological particles, *Phys. Fluids A* **1**, 101 (1989).

116. J. M. Occhialini, G. P. Muldowney, and J. J. L. Higdon, Boundary integral/spectral element approaches to the Navier–Stokes equations, *Int. J. Numer. Methods Fluids* **15**, 1361 (1992).

117. R.W. Ogden, *Non-linear Elastic Deformations* (Dover, New York, 1984).

118. Y. Pawar and K. J. Stebe, Marangoni effects on drop deformation in an extensional flow: The role of surfactant physical chemistry. I. Insoluble surfactants, *Phys. Fluids A* **8**, 1738 (1996).

119. H. L. G. Pina, J. L. M. Fernandes, and C. A. Brebbia, Some numerical integration forumulae over triangles and squares with a $1/R$ singularity, *Appl. Math. Modelling* **5**, 209 (1981).

120. H. Power, Low Reynolds number deformation of compound drops in shear flow, *Math. Methods Appl. Sci.* **16**, 61 (1993).

121. H. Power, A second kind of integral equation formulation for the Low Reynolds number interaction between a solid particle and a viscous drop, *J. Eng. Math.* **30**, 225 (1996).

122. H. Power, The interaction of a deformable bubble with a rigid wall at small Reynolds number: A general approach via integral equations, *Eng. Anal. Bound. Elem.* **19**, 291 (1997).

123. C. Pozrikidis, The flow of a liquid film along a periodic wall, *J. Fluid Mech.* **188**, 275 (1988).

124. C. Pozrikidis, The instability of a moving viscous drop, *J. Fluid Mech.* **210**, 1 (1990).

125. C. Pozrikidis, The deformation of a liquid drop moving normal to a plane wall, *J. Fluid Mech.* **215**, 331 (1990).

126. C. Pozrikidis, The axisymmetric deformation of a red blood cell in uniaxial straining flow, *J. Fluid Mech.* **216**, 231 (1990).

127. C. Pozrikidis, *Boundary Integral and Singularity Methods for Linearized Viscous Flow* (Cambridge Univ. Press, Cambridge, UK, 1992).

128. C. Pozrikidis, The buoyancy-driven motion of a train of viscous drops within a cylindrical tube, *J. Fluid Mech.* **237**, 627 (1992).

129. C. Pozrikidis, On the transient motion of ordered suspensions of liquid drops, *J. Fluid Mech.* **246**, 301 (1993).

130. C. Pozrikidis, Effects of surface viscosity on the deformation of liquid drops and the rheology of dilute emulsions in simple shearing flow, *J. Non-Newt. Fluid Mech.* **51**, 161 (1994).

131. C. Pozrikidis, Finite deformation of liquid capsules enclosed by elastic membranes in simple shear flow, *J. Fluid Mech.* **297**, 123 (1995).

132. C. Pozrikidis, Computation of periodic Green's functions of Stokes flow, *J. Fluid Math.* **30**, 79 (1996).

133. C. Pozrikidis, *Introduction to Theoretical and Computational Fluid Dynamics* (Oxford Univ. Press, New York, 1997).

134. C. Pozrikidis, Numerical studies of singularity formation at free surfaces and fluid interfaces in two-dimensional Stokes flow, *J. Fluid Mech.* **331**, 145 (1997).

135. C. Pozrikidis, The instability of a two-layer creeping flow in a channel with parallel-sided walls, *J. Fluid Mech.* **351**, 139 (1997).

136. C. Pozrikidis, *Numerical Computation in Science and Engineering* (Oxford Univ. Press, New York, 1998).

137. C. Pozrikidis, Numerical studies of cusp formation at fluid interfaces in Stokes flow, *J. Fluid Mech.* **357**, 29 (1998).

138. C. Pozrikidis, Gravity-driven flow of two adjacent layers through a channel and down a plane wall, *J. Fluid Mech.* **371**, 345 (1998).

139. C. Pozrikidis, *FDLIB* (*User Guide* San Diego, 1999).

140. C. Pozrikidis, Capillary instability and breakup of liquid threads, *J. Eng. Math.* **36**, 255 (1999).

141. C. Pozrikidis, A spectral-element method for particulate Stokes flow, *J. Comp. Phys.* **156**, 360 (1999).

142. C. Pozrikidis, Theoretical and computational aspects of the self-induced motion of three-dimensional vortex sheets, *J. Fluid Mech.*, in press (2000).

143. C. Pozrikidis, Three-dimensional oscillations of inviscid drops induced by surface tension, *Comput. Fluids*, in press (2000).

144. C. Pozrikidis, Effect of bending stiffness on the deformation of capsules in simple shear flow, submitted for publication (2000).

145. C. Pozrikidis and S. T. Thoroddsen, The deformation of a liquid film flowing down an inclined plane wall over a small particle arrested on the wall, *Phys. Fluids A* **11**, 2546 (1991).

146. A. R. M. Primo, L. C. Wrobel, and H. Power, An indirect boundary element method for slow viscous flow in a bounded region containing air bubbles, *J. Eng. Math.* **37**, 305 (2000).

147. A. R. M. Primo, L. C. Wrobel, and H. Power, Boundary integral formulation for slow viscous flow in a deforming region containing a solid inclusion, *Eng. Anal. Bound. Elem.* **24**, 53 (2000).

148. J. M. Rallison, A numerical study of the deformation and burst of a viscous drop in general shear flows, *J. Eng. Mech.* **109**, 465 (1981).

149. J. M. Rallison and A. Acrivos, A numerical study of the deformation and burst of a viscous drop in an extensional flow, *J. Eng. Mech.* **89**, 191 (1978).

150. S. Ramanujan and C. Pozrikidis, Deformation of liquid capsules enclosed by elastic membranes in simple shear flow: Large deformations and the effect of fluid viscosities, *J. Fluid Mech.* **361**, 117 (1998).

151. E. Reissner, On the theory of thin elastic shells, in *Contributions to Applied Mechanics*, H. Reissner Anniversary Volume, edited by J. W. Edwards (Ann Arbor, 1949), p. 231.

152. E. Reissner, On axisymmetrical deformations of thin shells of revolution, *in Proceedings, Third Symposium in Applied Mathematics* (1950), p. 27.

153. E. Reissner, On the equations for finite symmetrical deflections of thin shells of revolution, in *Progress in Applied Mechanics*, Prager Anniversary Volume (McMillan, New York, 1963), p. 171.

154. E. Reissner, On finite symmetrical deflections of thin shells of revolution, *J. Appl. Mech.* **36**, 267 (1969).

155. J. Roumeliotis and G. R. Fulford, Droplet interactions in creeping flow, *Comput. Fluids* **29**, 435 (2000).

156. C. E. Rosenkilde, Surface-energy tensors, *J. Math. Phys.* **8**, 84 (1967).

157. J. L. Sanders, Nonlinear theories of thin shells, *Quart. Appl. Mech.* **21**, 21 (1963).

158. A. S. Sangani and G. Mo, An $O(N)$ Algorithm for Stokes and Laplace interactions of particles, *Phys. Fluids* **8**, 1990 (1996).

159. T. Sapir and A. Nir, A hydrodynamic study of the furrowing stage during cleavage, *PCH PhysicoChem. Hydrodyn.* **6**, 803 (1985).

160. A. D. Schleixer and R. T. Bonnecaze, Displacement of a two-dimensional immiscible droplet adhering to a wall in shear and pressure-driven flows, *J. Fluid Mech.* **383**, 29 (1999).

161. l. E. Scriven, Dynamics of a fluid interface, *Chem. Eng. Sci.* **12**, 803 (1985).

162. T. W. Secomb and R. Skalak, Surface flow of viscoelastic membranes in viscous fluids, *Q. J. Mech. Appl. Math.* **35**, 233 (1982).

163. U. Seifert, Configurations of fluid membranes and vesicles, *Adv. Phys.* **46**, 13 (1997).

164. U. Seifert, Modelling nonlinear red cell elasticity, *Biophys. J.* **75**, 1141 (1998).

165. S. J. Sherwin and G. E. Karniadakis, A triangular spectral element method—Applications to the incompressible Navier–Stokes equations, *Comput. Methods Appl. Mech. Eng.* **123**, 189 (1995).

166. J. G. Simmonds and D. A. Danielson, Nonlinear shell theory with finite rotation and stress-function vectors, *J. Appl. Mech.* **39**, 1098 (1972).

167. R. Skalak, N. Özkaya, and T. C. Skalak, Biofluid mechanics, *Annu. Rev. Fluid Mech.* **21**, 167 (1989).

168. R. Skalak, A. Tözeren, P. R. Zarda, and S. Chien, Strain energy function of red blood cell membranes, *Biophys. J.* **13**, 245 (1973).

169. V. Sladek and J. Sladek, *Singular Integrals in Boundary Element Methods* (Computational Mechanics Publications, Southampton, 1998).

170. J. C. Slattery, *Interfacial Transport Phenomena* (Springer-Verlag, Berlin, 1990).

171. D. J. Steigmann, On the relationship between the Cosserat and Kirchhoff–Love theories on elastic shells, *Math. Mech. Solids* **4**, 275 (1999).

172. D. J. Steigmann, Fluid films with curvature elasticity, *Arch. Rat. Mech.* **150**, 127 (1999).

173. D. J. Steigmann and R. W. Ogden, Plane deformations of elastic solids with intrinsic boundary elasticity, *Proc. R. Soc. London Ser. A* **453**, 853 (1997).

174. D. J. Steigmann and R. W. Ogden, Elastic surface substrate interactions, *Proc. R. Soc. London Ser. A* **455**, 437 (1999).

175. H. A. Stone, A simple derivation of the time-dependent convection-diffusion equation for surfactant transport along a deforming interface, *Phys. Fluids A* **2**, 111 (1990).

176. H. A. Stone, Drop deformation and breakup in viscous flows, *Annu. Rev. Fluid Mech.* **26**, 605 (1994).

177. H. A. Stone and L. G. Leal, Relaxation and breakup of an initially extended drop in an otherwise quiescent fluid, *J. Fluid Mech.* **198**, 399 (1989).

178. H. A. Stone and L. G. Leal, The influence of initial deformation on drop breakup in subcritical time-dependent flows at low Reynolds numbers, *J. Fluid Mech.* **206**, 223 (1989).

179. H. A. Stone and L. G. Leal, Breakup of concentric double emulsion droplets in linear flows, *J. Fluid Mech.* **211**, 123 (1990).

180. H. A. Stone and L. G. Leal, The effects of surfactants on drop deformation and breakup, *J. Fluid Mech.* **222**, 161 (1990).

181. J. A. Stoos and L. G. Leal, Particle motion in axisymmetric stagnation flow toward an interface, *AIChE J.* **35**, 196 (1989).

182. J. A. Stoos and L. G. Leal, A spherical particle straddling a fluid/gas interface in an axisymmetric straining flow, *J. Fluid Mech.* **217**, 263 (1990).

183. G. T. Symm, Integral equation methods in potential theory, II. *Proc. R. Soc. London Ser. A* **275**, 33 (1963).

184. J. Tanzosh, M. Manga, and H. A. Stone, Boundary integral methods for viscous free-boundary problems: Deformation of single and multiple fluid-fluid interfaces, in *Boundary Element Technology VI*, edited by C. A. Brebbia and M. S. Ingber (Elsevier, Amsterdam, 1992), p. 19.

185. M. Tjahjadi, H. A. Stone, and J. M. Ottino, Satellite and subsattelite formation in capillary breakup, *J. Fluid Mech.* **243**, 297 (1992).

186. E. M. Toose, D. Van Den Ende, B. J. Geurts, J. G. M. Kuerten, and P. J. Zandbergen, Axisymmetric non-Newtonian drops treated with a boundary integral method, *J. Eng. Math.* **30**, 131 (1996).

187. T. M. Tsai and M. J. Miksis, The effects of surfactant on the dynamics of bubble snap-off, *J. Fluid Mech.* **337**, 381 (1997).

188. S. J. Uijttewaal, E. Nijhof, and R. M. Heethaar, Droplet migration, deformation, and orientation in the presence of a plane wall: A numerical study compared with analytical theories, *Phys. Fluids A* **5**, 819 (1993).

189. S. J. Uijttewaal and E. Nijhof, The motion of a droplet subjected to linear shear flow including the presence of a plane wall, *J. Fluid Mech.* **302**, 45 (1995).

190. G. A. L. Van de Vorst, Integral method for a two-dimensional Stokes flow with shrinking holes applied to viscous sintering, *J. Fluid Mech.* **257**, 667 (1993).

191. G. A. L. Van de Vorst, *Modelling and Numerical Simulation of Viscous Sintering*, doctoral dissertation (University of Technology, Eindhoven, 1994).

192. G. A. L. Van de Vorst, Integral formulation to simulate the viscous sintering of a two-dimensional lattice of periodic unit cells, *J. Eng. Math.* **30**, 97 (1996).

193. A. M. Waxman, Dynamics of a couple-stress fluid membrane, *Stud. Appl. Math.* **70**, 63 (1984).

194. H. Wong, D. Rumschitzki, and C. Maldarelli, On the surfactant mass balance at a deforming fluid interface, *Phys. Fluids A* **8**, 3203 (1996).

195. H. Wong, D. Rumschitzki, and C. Maldarelli, Theory and experiment on the low-Reynolds-number expansion and contraction of a bubble pinned at a submerged tube tip, *J. Fluid Mech.* **356**, 93 (1998).

196. H. Wong, D. Rumschitzki, and C. Maldarelli, Marangoni effects on the motion of an expanding or contracting bubble pinned at a submerged tube tip, *J. Fluid Mech.* **379**, 279 (1999).

197. D. Y. K. Yap and D. P. Gaver III, The influence of surfactant on two-phase flow in a flexible-walled channel under bulk equilibrium conditions, *Phys. Fluids* **10**, 1846 (1998).

198. S. Yon and C. Pozrikidis, A finite-volume/boundary-element method for flow past interfaces in the presence of surfactants, with application to shear flow past a viscous drop, *Comput. Fluids* **27**, 879 (1998).

199. S. Yon and C. Pozrikidis, Deformation of a liquid drop adhering to a plane wall: Significance of the drop viscosity and the effect of an insoluble surfactant, *Phys. Fluids* **11**, 1297 (1999).

200. G. K. Youngren and A. Acrivos, Stokes flow past a particle of arbitrary shape: A numerical method of solution, *J. Fluid Mech.* **69**, 377 (1975).

201. G. K. Youngren and A. Acrivos, On the shape of a gas bubble in a viscous extensional flow, *J. Fluid Mech.* **76**, 433 (1976).

202. P. R. Zarda, S. Chien, and S. Skalak, Elastic deformations of red blood cells, *J. Biomech.* **10**, 211 (1977).

203. D. F. Zhang and H. A. Stone, Drop formation in viscous flows at a vertical capillary tube, *Phys. Fluids* **9**, 2234 (1997).

204. H. Zhou and R. H. Davis, Axisymmetric thermocapillary migration of two deformable viscous drops, *J. Colloid Interface Sci.* **181**, 60 (1996).

205. H. Zhou and C. Pozrikidis, The flow of suspensions in channels: Single files of drops, *Phys. Fluids A*, **5**, 311 (1993).

206. H. Zhou and C. Pozrikidis, The flow of ordered and random suspensions of liquid drops in a channel, *J. Fluid Mech.* **255**, 103 (1993).

207. H. Zhou and C. Pozrikidis, Pressure-driven flow of suspensions of liquid drops, *Phys. Fluids* **6**, 80 (1994).

208. H. Zhou and C. Pozrikidis, Deformation of liquid capsules with incompressible interfaces in simple shear flow, *J. Fluid Mech.* **283**, 175 (1995).

209. A. Z. Zinchenko and R. H. Davis, An efficient algorithm for hydrodynamical interaction of many deformable drops, *J. Comput. Phys.* **157**, 539 (2000).

210. A. Z. Zinchenko, M. A. Rother, and R. H. Davis, A novel boundary-integral algorithm for viscous interaction of deformable drops, *Phys. Fluids* **9**, 1493 (1997).

211. A. Z. Zinchenko, M. A. Rother, and R. H. Davis, Cusping, capture and breakup of interacting drops by a curvatureless boundary-integral algorithm, *J. Fluid Mech.* **391**, 249 (1999).

212. D. Zinemanas and A. Nir, On the viscous deformation of biological cells under anisotropic surface tension, *J. Fluid Mech.* **193**, 217 (1988).

213. D. Zinemanas and A. Nir, Surface viscoelastic effects in cell cleavage, *J. Biomech.* **23**, 417 (1990).

214. D. Zinemanas and A. Nir, A fluid-mechanical model of deformation during embryo exogastrulation, *J. Biomech.* **25**, 341 (1992).